ISOTOPIC COMPOSITION OF PRECIPITATION IN A TOPOGRAPHICALLY COMPLEX, SEASONALLY SNOW-DOMINATED WATERSHED: HYDROMETEOROLOGICAL CONTROLS AND VARIATIONS FROM THE GLOBAL METEORIC WATER LINE

by

Daniel J. Tappa

A thesis

submitted in partial fulfillment

of the requirements for the degree of

Master of Science in Hydrologic Sciences

Boise State University

May 2013

BOISE STATE UNIVERSITY GRADUATE COLLEGE

DEFENSE COMMITTEE AND FINAL READING APPROVALS

of the thesis submitted by

Daniel J. Tappa

Thesis Title: Isotopic Composition of Precipitation in a Topographically Complex, Seasonally Snow-Dominated Watershed: Hydrometeorological Controls and Variations from the Global Meteoric Water Line

Date of Final Oral Examination: 13 March 2013

The following individuals read and discussed the thesis submitted by student Daniel J. Tappa, and they evaluated his presentation and response to questions during the final oral examination. They found that the student passed the final oral examination.

Alejandro Flores, Ph.D.	Chair, Supervisory Committee
Shawn Benner, Ph.D.	Member, Supervisory Committee
James McNamara, Ph.D.	Member, Supervisory Committee
Matthew Kohn, Ph.D.	Member, Supervisory Committee

The final reading approval of the thesis was granted by Alejandro Flores, Ph.D., Chair of the Supervisory Committee. The thesis was approved for the Graduate College by John R. Pelton, Ph.D., Dean of the Graduate College.

ACKNOWLEDGEMENTS

First and foremost I would like to thank my Supervisory Committee chair, Dr. Alejandro “Lejo” Flores, who took me in under abnormal circumstances and provided critical support to me throughout the process. Quite simply, without his knowledge, motivation, and patience this thesis would not have been possible. I would also like to thank the members of my Supervisory Committee, Professor Shawn Benner, Professor James McNamara, and Professor Matthew Kohn for their expertise and support of my thesis work. I owe additional gratitude to Professor Matthew Kohn for the use of his Stable Isotope Laboratory at Boise State University, and to Research Scientist Samantha Evans for her advice throughout the thesis process and assistance in the lab and in the field. I would also like to thank Kimberly Smith for helping with lab sample preparation.

This thesis project culminated in the collection of several hundred precipitation samples and I would like to thank Pam Aishlin and Patrick Kormos for their assistance with field work in Dry Creek Experimental Watershed. I would like to acknowledge the financial support provided by the Geosciences Department at Boise State University and the NSF GK-12 Fellowship. Also, the NSF GK-12 Fellowship program provided me with an amazing teaching experience and has better prepared me for my professional career. I would like to acknowledge everyone I worked with at the Boise WaterShed and Foothills Learning Center, your support has been critical to the completion of my thesis. Last, the love and support of my family has been immeasurable to me during this process.

ABSTRACT

The stable isotope composition of water ($\delta^{18}O$ and $\delta^{2}H$) can reveal important hydrometeorologic and hydroclimatic information. For instance, simultaneous measurement of the stable isotope composition of precipitation and stream water is used to estimate the distribution of hydrologic transit time in catchments, which can provide information about hydrologic flow paths, storage, and source water. However, in mountain watersheds characterized by large topographic relief, the spatiotemporal distribution of precipitation can vary dramatically, as can the isotopic composition of precipitation. Compounding this variability is the transition in precipitation phase from rain to snow, which can markedly affect isotopic compositions of precipitation. This study aims to improve the use of stable isotope methods for hydrologic investigations in complex terrain by investigating the hydrometeorological and spatial controls on the isotopic composition of precipitation, along with improving our understanding of the spatial variability and evolution of the isotopic composition of snow. Additionally, we constructed a seasonally weighted local meteoric water line (LMWL) for the Treasure Valley of southwestern Idaho, which is expressed by the equation $\delta^{2}H = 7.40*\delta^{18}O - 2.17$. The LMWL of the greater-Boise area is considerably influenced by the semiarid climate of southwest Idaho, yielding a slope and y-intercept lower than the global meteoric water line (GMWL: $\delta^{2}H = 8*\delta^{18}O + 10$). Moderate to strong statistically significant ($p < 0.05$) correlations exists between several hydrometeorological variables (e.g., surface air temperature, relative humidity, precipitation amount, precipitation

intensity) and the isotopic composition of precipitation from individual events. A very strong negative correlation ($r = -0.98$, $p < 0.02$) exists between the amount-weighted isotopic composition of precipitation and the elevation from individual collection sites (Altitude effect lapse rate: -2.2‰/km). Snow sampling campaigns revealed significant variability in the spatial distribution of the isotopic composition of snow. $\delta^{18}O$ of bulk snow core samples varied between -16 and -19 ‰ in an area covering 256 m^2 at the Treeline study site in Dry Creek Experimental Watershed, which is greater than the variation of the annual $\delta^{18}O$ of Dry Creek stream water. Revised methods for characterizing the input signal for transit time estimation (e.g., sampling snowmelt lysimeter water, applying Altitude effect lapse rate to isotopic composition of precipitation) will more accurately represent isotope tracers arriving in watersheds as precipitation and leaving as streamflow.

TABLE OF CONTENTS

LIST OF FIGURES

LIST OF TABLES

LIST OF ABBREVIATIONS

BSU	Boise State University
GC	Graduate College
TDC	Thesis and Dissertation Coordinator
GMWL	Global Meteoric Water Line
LMWL	Local Meteoric Water Line
DCEW	Dry Creek Experimental Watershed
NAM	North American Mesoscale Model
LCL	Lifted Condensation Level
LWIA	Liquid Water Isotope Analyzer
VSMOW	Vienna Standard Mean Ocean Water

CHAPTER ONE: VARIABILITY OF THE ISOTOPIC COMPOSITION OF PRECIPITATION

1. Introduction

Physical water scarcity is affecting approximately one fifth of the world's population, while water withdrawals are predicted to increase by 50 percent by 2025 in developing countries, and 18 percent in developed countries (Moe and Rheingans 2006). In a world where climate warming and population growth are putting unprecedented pressures on hydrologic systems, there is a critical need to better quantify the size and rates of movement between and among natural and man-made reservoirs of water. This is particularly true in the semiarid regions of the western United States, which is characterized by increasing water demand and water scarcity.

A variety of tools are available to characterize these hydrologic reservoirs, although each tool is associated with strengths and weaknesses. The stable isotopes of water are a particularly powerful natural environmental tracer and have been used as a tool to investigate hydrologic processes for several decades (Clark and Fritz 1997). Stable isotopes of water are typically not subject to change during interaction with subsurface material, making them an ideal tracer of hydrologic processes. Water molecules with enriched isotopes (HDO, $H_2{}^{18}O$) tend to be relatively concentrated in the more condensed phase of water, which causes small differences in $^{2}H/^{1}H$ and $^{18}O/^{16}O$ ratios of water molecules between phases in the hydrologic cycle.

The use of stable isotopes of water in catchment hydrology has improved our understanding of transit time, which is a crucial hydrologic parameter that contains integrated information about flow-paths, storages times, and source water (Henderson-Sellers et al. 2004, McGuire and McDonnell 2006). The stable isotope composition of meteoric water can be used to model atmospheric circulation and can reveal information regarding moisture sources (Kirby et al. 2002), while the stable isotope composition of ice-cores is used to reconstruct and analyze past climate variability (Dansgaard et al. 1993, Petit et al. 1999).

Recent technological advances have made measurements of stable isotopes of water far more economical than historical averages. Laser-based methods, specifically the Cavity Ring-Down Spectroscopy technique, for measuring water isotopes has resulted in more efficient and significantly cheaper sample processing relative to the former isotope ratio mass spectrometer techniques (Brand et al. 2009). Increased efficiency of water isotope measurements enables broader sampling in space and time, and facilitates improved characterization of hydrologic flow paths and reservoirs. As a result, the use of isotopes in hydrologic studies has expanded significantly (Berman et al. 2009); however, more measurements also reveal complexity in the patterns of inferred hydrologic processes.

1.1 Isotope Fractionation and Meteoric Water Lines

Isotopic fractionation, which causes variations in the isotopic composition of water, is associated with phase transitions of water between different water reservoirs in the hydrologic cycle and diffusion during transport. Two types of fractionation occur in the hydrologic cycle. Equilibrium fractionation is the partitioning of isotopes between

two phases of water that are at chemical equilibrium (water vapor condensing to liquid water), and is driven by differences in bonding energies (Pfahl and Wernli 2008). Generally, isotopes with an increased mass (enriched) form stronger bonds, thus it requires more energy to break the bond of an enriched isotope relative to a depleted isotope. This fractionation process is highly temperature dependent and decreased temperatures result in greater fractionation between isotopes whereas high temperatures result in littler fractionation between isotopes. Kinetic fractionation, or non-equilibrium fractionation, is a mass dependent partition between isotopes during a unidirectional process (Kendall and McDonnell 1998). A classic example of this type of fractionation is the evaporation of water. Water molecules with ^{16}O and ^{1}H evaporate more readily than molecules with ^{18}O and ^{2}H. Evaporation processes result in the isotopic composition of the source (surface water and soil moisture) enriched with ^{18}O and ^{2}H relative to the more depleted evaporated atmospheric water vapor, but with a different functional relationship than for equilibrium fractionation.

In general, the more depleted isotopes react faster and end up relatively concentrated in the products of a reaction relative to enriched isotopes (Craig and Gordon 1965, Merlivat and Jouzel 1979). The resulting partitioning between phases in the hydrologic cycle is why the isotopic composition of water can be used to trace hydrologic processes (Lee et al. 2007). The nature of the hydrologic cycle complicates the use of stable isotopes to trace hydrologic processes. Precipitation arriving at one location often contains meteoric water from numerous moisture source locations. To improve the accuracy and value of information contained in measurements of the stable isotopes of

water in catchment studies, it is crucial to investigate the causes of spatial and temporal variations of the isotopic composition of precipitation.

The isotopic composition of hydrogen and oxygen are reported in delta (δ) notation, expressing a per mil deviation from a standard and defined as,

$$\delta^{18}O\ ‰ = (R_{sample}/R_{standard} - 1) * 1000 \quad (1)$$

where R_{sample} and $R_{standard}$ are the $^{18}O/^{16}O$ ratios in the sample and the standard respectively. The isotopic composition of hydrogen is reported in the same format (replacing $^{18}O/^{16}O$ in Equation 1 with $^{2}H/^{1}H$). By convention, $\delta^{18}O$ and $\delta^{2}H$ of ocean water is 0.

Systematically, the fractionation processes that affect the stable hydrogen and oxygen isotopes are similar, which results in comparable behavior between isotopic species within the hydrologic cycle (Friedman 1953). This relationship is expressed in the global meteoric water line (GMWL, Figure 1). The GMWL was first derived by Craig (1961) by analyzing the isotopic composition of meteoric water samples collected around the world by the International Atomic Energy Agency (IAEA) and is expressed as:

$$\delta D = 8.13\ \delta^{18}O + 10.8 \quad (2)$$

Equilibrium fractionation processes that affect water isotopes are ~8 times greater for hydrogen than oxygen, resulting in the slope of ~8 for the GMWL as displayed in Equation 2 (Pfahl and Wernli 2008). This is because the fractionation processes are

controlled by differences in vibrational frequencies of affected bonds, with the greater differences in mass causing the greatest fractionation. Deuterium (^{2}H) has double the mass of ^{1}H, while the mass of ^{18}O is only 13% greater than ^{16}O, which results in fractionation processes affecting hydrogen more than oxygen. Because the average isotopic composition of oceanic water is 0, the y-intercept of 10.8 of the GMWL reflects the fact that meteoric water and oceanic water are not in thermodynamic equilibrium (Pfahl and Wernli 2008).

The GMWL integrates the worldwide isotopic composition of meteoric water (i.e., precipitation); therefore, it serves as a useful baseline against which isotope measurements from the various reservoirs of the hydrologic cycle can be compared. The extent to which measurements depart from the GMWL can provide important insight into the presence and strength of hydrologic processes, such as evaporation, that lead to non-equilibrium fractionation such as evaporation. However, the stable isotope composition of local meteoric water may vary from the GMWL. Therefore, a local meteoric water line (LMWL) can exhibit a different slope and y-intercept than the GMWL.

As a result of potential variability between the GMWL and the LMWL of a specific region, isotope comparison studies are often only useful if measurements depart or align with the LMWL. The major processes controlling the variability between GMWLs and LMWLs are the humidity during primary transport after evaporation and secondary evaporation after precipitation falls from a cloud, which is typical of arid climates. In general, complex atmospheric processes are the reason why the isotopic composition of precipitation varies on an event scale basis.

1.2 Atmospheric Controls

Past studies have identified seasonality of precipitation (Dansgaard 1964, Lee et al. 2003, Dutton et al. 2005), water source surface temperature (Craig 1961, Dansgaard 1964), precipitation amount (Dansgaard 1964), elevation (Poage and Chamberlain 2001), latitude (Dansgaard 1964, Fricke and O'Neil 1999), and air mass history (Lawrence et al. 1982, Burnett et al. 2004) as significant determining factors in the isotopic composition of precipitation (Sjostrom and Welker 2009). The continental effect is the observation of the depletion of enriched isotopes in water vapor the farther away air-masses are from coastal regions (Figure 2). This follows a Rayleigh distillation process, resulting in the isotopic composition of precipitation becoming more depleted the farther a precipitating air-mass moves inland (Dansgaard 1964). The Rayleigh distillation model, however, does not account for below cloud secondary evaporation, which can further enrich precipitating meteoric water, leading to inaccurate predictions of the isotopic composition of precipitation (Peng et al. 2007). Most of these factors are understood on long-term and large-scale studies, while very little work has been done to understand how dynamic physical processes affect the stable isotope composition of precipitation on an intra-seasonal and catchment scale.

1.3 Transit Time Estimation and Input Characterization Problem

Transit time is the amount of time elapsed between the input and output of water in a flow system, thus the distribution of catchment transit times is a fundamental catchment descriptor and reveals critical hydrologic processes in a single characteristic (McGuire and McDonnell 2006). Transit time distributions can be determined experimentally by simultaneously characterizing the stable isotope composition of

precipitation input to a catchment as well as the stream water exiting. Part of the usefulness of stable isotopes is that they are naturally occurring tracers that are applied to catchments during precipitation events and transported to stream channels through surface and subsurface processes. The stable isotope composition of the water at the catchment stream outlet reveals a distribution that is damped and lagged compared to the applied input signal due to differential transport (McGuire and McDonnell 2006, McDonnell et al. 2010). Through the use of a convolution integral, catchment transit time distributions can be fit. Since the stable isotope composition of water is not a dissolvable or exchangeable ion like many tracers, it serves as a conservative tracer.

A major problem in catchment transit time modeling, outlined by a conceptual model in Figure 3, is the characterization of the input stable isotope signal for transit time estimation models. The stable isotope composition of precipitation (as well as the total volume of precipitation input) is rarely homogenous over the extent of the catchment, particularly as the scale of the catchment increases. Moreover, large spatial and temporal variability in the stable isotope composition of precipitation would also be expected in watersheds with large topographic relief and/or spanning the rain-snow transition, because of the corresponding temperature gradients that control fractionation processes. Figure 3 also depicts the annual variability of the $\delta^{18}O$ composition of precipitation at two locations differing in elevation in the same catchment. The variability of the isotopic composition of precipitation between the two locations is greater than the corresponding annual variability of the $\delta^{18}O$ composition of the stream water output from the same catchment.

McGuire and McDonnell (2006) tracked the variability of the isotopic composition of precipitation for 3 storm events at Lookout Creek Watershed (Figure 4), and highlighted how the isotopic composition of precipitation is elevation and storm-track dependent. During orographic lift, isotopically enriched water molecules tend to condense and precipitate more readily than water molecules with depleted isotopes, leaving the subsequent water vapor more isotopically depleted. Correspondingly, adiabatic cooling during orographic lift further depletes the isotopic composition of subsequent precipitation due to decreased temperature during condensation (equilibrium fractionation).

These factors drive the altitude effect, which is the depletion of the isotopic composition of precipitation with increasing elevation (Dansgaard 1964). Typical gradients are -0.15 to -0.5 ‰ per 100 meters for $\delta^{18}O$, and -1.5 to -4 ‰ per 100 meters for $\delta^{2}H$ (Ambach et al. 1968). In watersheds of sufficient size, the continental effect can simultaneously impact the isotope composition of precipitation. The isotopic composition of precipitation at a location, therefore, is influenced by a variety of simultaneously acting processes operating at a range of spatial and temporal scales.

These aforementioned factors complicate the input signal for transit time characterizing in complex terrain, necessitating care when measuring the isotopic composition of precipitation to estimate the distribution of catchment travel times. The assumption in transit time studies that the stable isotope composition of precipitation is a homogenous input to catchments, especially in complex terrain, is flawed. Furthermore, even if a net input stable isotope composition signal can be determined, the use of a

convolution integral implicitly assumes that the travel time distribution is time invariant and that the output stable isotope composition is linearly related to the input composition.

1.4 Study Objectives

The objective of this study is to improve the understanding of the hydrometeorological and spatial controls on the isotopic composition of precipitation in mid-continent watersheds where multiple factors control the isotopic composition of meteoric water. The location of this investigation took place in Dry Creek Experimental Watershed (DCEW) near Boise, ID. Improved characterization of these controls on the stable isotope composition of precipitation will increase our ability to understand and predict the spatiotemporal variability of the isotopic composition of precipitation at the catchment scale. This improved understanding will correspondingly enhance our ability to characterize the input stable isotope function for, and estimation of, travel time distributions in watersheds in complex terrain. To facilitate the comparison of stable isotope compositions in precipitation in our study region, we must first construct a LMWL for the greater-Boise area of southwestern Idaho. The LMWL will also be a useful baseline for future and ongoing hydrologic studies in the region (e.g., determining sources of groundwater recharge, surface and groundwater interaction, water-mineral exchange, plant source water, etc.).

To fulfill these objectives, we analyzed correlations between the isotopic composition of precipitation from individual events and corresponding hydrometeorlogical variables (e.g., temperature, relative humidity, precipitation amount, storm duration, etc.) from the same events. Potential moisture source locations and the locations where air masses made landfall were also investigated for 30 precipitation

events in 2011 and 2012, along with the connectivity between specific landfall locations and the isotopic composition of precipitation. Additionally, we created a precipitation collection network throughout the Treasure Valley of southwestern Idaho to obtain a spatial range of samples for the construction of a LMWL.

2. Site Description

The Treasure Valley is located in the western Snake River Plain in southwest Idaho. The valley is mostly below 1000 m Mean Sea Level (MSL) in elevation, and is bordered by the Boise Front Mountains to the northwest and the Owyhee Mountains to the southwest, each with mountain peaks reaching 2400 m MSL. Southwest Idaho is classified as a BSk climate by the Köppen Climate Classification System (Henderson-Sellers and Robinson 1986). The BSk category is associated with semiarid mid-latitude climates where potential evaporation exceeds precipitation, and weather is transitional between deserts and humid climates. To the west, the Blue Mountains and Cascade Range of Oregon significantly affect Pacific Maritime air masses as they move east towards the Treasure Valley. As a result of orographic lifting, air masses are considerably drier when they arrive in the Treasure Valley from the west and northwest.

The climate in the region reflects dynamic interactions between contrasting North Pacific High and Aleutian Low systems (Bograd et al. 2002). During the winter months, the Aleutian Low (positioned in the Gulf of Alaska near the Aleutian Islands) generates storms, and migratory low pressure systems move towards the Pacific Northwest coast, bringing abundant moisture. During the summer months, the Aleutian Low migrates toward the North Pole and diminishes significantly in intensity, and the North Pacific High system dominates weather in the region. The North Pacific High results in clear and

dry conditions and typically establishes in June and lasts through September. On average, the lower elevations of southwest Idaho receive roughly 300 mm of annual precipitation, with less than 50 mm falling between June and October (National Weather Service 2012). Significantly greater annual precipitation falls in mountains surrounding the Treasure Valley due to orographic lift.

Dry Creek Experimental Watershed (DCEW) is a small research catchment (~28 km^2) in the foothills near Boise, ID. Elevation varies between approximately 1100 m at the intersection of Dry Creek and Bogus Basin Road and 2200 m at the headwaters near Bogus Basin Ski Area (McNamara et al. 2005). Dry Creek is a perennial stream and a tributary of the Boise River. Precipitation in the watershed is winter dominate, with lower elevations typically receiving rain while upper elevations receive mostly snow. The elevation gradient is associated with a significant orographic effect, with an average 250 mm increase in mean annual precipitation between 1080 and 1850 m. Similar to the seasonality of precipitation in the surrounding valleys of southwest Idaho, the majority of precipitation falls between October and June in the higher elevations of DCEW, with roughly 8% of the total annual precipitation occurring during the summer months of June, July, and August in 2010 and 2011. A more thorough description of the watershed can be found by Smith et al. 2011 and Aishlin and McNamara 2011.

2.1 Methods

Precipitation was manually collected on an event-scale basis at 10 sites in the western Snake River Plain from July 2011 through June 2012 (Figure 5). Additionally, precipitation at 4 study sites within DCEW was collected on an event-scale basis between September 2008 and June 2012 (Figure 6). Altogether, 393 samples were collected from

14 sites using an apparatus consisting of 32 ounce funnels on top of 250 ml opaque beakers, with small sections of 8 inch diameter opaque PVC pipe serving as the base. Snow was collected from the top of the funnels and from snow-boards. Snow-boards are flat 2 ft. x 1 ft. boards with a pipe attached to the center of the board. After each snow event, snow is removed from the board and the board is raised to the top of the snowpack so additional snow accumulated on top of the board.

Precipitation collection took place within 24 hours after the conclusion of storm events to minimize evaporative enrichment. Additionally, to assess the potential impacts of evaporative enrichment on samples, a controlled enrichment experiment was performed during the summer of 2012. The evaporation enrichment experiment did not show any substantial alterations to the isotopic composition of the sample water (Figure 7).

During collection, liquid water samples were transferred and stored in 5 ml vials with inverted caps. Solid water samples were sealed in plastic bags and melted in a refrigerator. After the solid samples were completely melted, the samples were well mixed and transferred into 5 ml vials. All samples were stored at room temperature until isotopic analysis was performed

Stable isotope analysis took place using a Los Gatos Research, Inc. Liquid Water Isotope Analyzer (LWIA) in the Stable Isotope Laboratory in the Department of Geosciences at Boise State University. The LWIA is a fourth generation cavity enhanced adsorption ring-down spectrometer, and allows for the processing of several hundred samples per day. Each sample was transferred from 5 ml storage vials to 2 ml vials used by the LWIA by using graduated 3 ml large bulb pipets. A new pipet was used for the

transfer of every sample to avoid isotope cross-contamination. Our methods are largely consistent with previous studies (Goldsmith et al. 2011, Welker 2000) and USGS sampling protocol.

Each sample is measured through 6 injections, and the average and standard deviation of the final 4 measurements of the oxygen and hydrogen isotopic composition reported for each sample. The first 2 injections are excluded from analysis to minimize the possibility of contamination from the previous sample injections. Samples are calibrated to the international Vieanna Standard Mean Ocean Water (VSMOW) standard using a suite of five reference waters ranging is isotopic composition between -2.96 and -19.57 ‰ $\delta^{18}O$, -9.8 and -154.1 ‰ $\delta^{2}H$. The LWIA is calibrated with these reference materials during each sample run allowing for variable operating conditions.

The isotopic composition of all samples used in this study is displayed in Table 1, while Table 2 displays the average isotopic composition, the number of samples, and the elevation (MSL) for each site location. Most of sample collection occurred at the 4 highest elevation sites, which correspond to the 4 study sites in DCEW. The guaranteed precision error is 0.2‰ for $\delta^{2}H$ and 0.03‰ for $\delta^{18}O$, with a typical precision range of 0.15‰ for $\delta^{2}H$ and 0.02‰ for $\delta^{18}O$.

2.2 Weather Data and NOAA HYSPLIT Model

Hydrometeorological data were collected for the 30 largest precipitation events from May 2011 through May 2012 at 3 study sites within DCEW that are co-located with research-grade weather stations. Hourly hydrometeorological data were collected and averaged for the duration of each event. The duration of a continuous storm event was considered to be the period of continuous precipitation accumulation, allowing for breaks

in hourly precipitation no longer than 12 hours. Storm duration ranged from 5 hours to 72 hours using this criterion. We used the 12 hour criterion because the obtained durations often coincided with when samples were collected, and collection typically occurred after precipitation had completely ended and more precipitation was not in the immediate forecast. The retrieved hydrometeorological data for each event consisted of surface temperature, relative humidity, wind speed, wind direction, storm duration, duration of accumulating hours of precipitation, and precipitation amount. These data were collected because they are related to the atmospheric processes that are thought to affect the stable isotope composition of precipitation (Sjostrom and Welker 2009).

We used the NOAA HYSPLIT model (Draxler and Rolph 2003) air parcel reverse trajectory technique to determine where air masses originate and entered the west coast of the United States and Canada for each precipitation event. The HYSPLIT model has been used to track the dispersion of aerosols on a regional scale, but can also be used to determine water vapor sources (Strong et al. 2007, Breitenbach et al. 2010). The North American Mesoscale Model (NAM) 12 km reanalysis dataset (Rogers et al. 2005) was used to force the HYSPLIT model, resulting in the HYSPLIT model using NAM 3-dimensional wind velocity fields to advance air parcels (either forward or backward in time) through the 12 km grid. Additional inputs required to run the model are starting time of model run, starting elevation, and vertical motion.

The starting time of each run was determined by the onset of precipitation at the DCEW Treeline weather stations for all 30 events. Starting elevation of the reverse trajectory runs were the lifted condensation level (LCL) for each event, which was obtained from atmospheric sounding data from the Boise National Weather Service office

for the sounding immediately before precipitation onset. Since soundings are only performed twice daily (at 00z and 12z), the potential lag time between the sounding and the onset of precipitation introduces some uncertainty into the inferred location of the LCL. The model vertical velocity option was used for the vertical motion input, resulting in NAM vertical velocities used to simulate vertical motion.

3. Results and Discussion

The following section describes the local meteoric water line for the Treasure Valley region, along with our analysis of correlations between the stable isotope composition of individual precipitation events, hydrometeorological variables, and potential precipitation moisture sources. In the first subsection, we discuss variations from the GMWL and the local climatic conditions with which these variations are associated. The second subsection highlights correlations between hydrometeorological variables and the isotopic composition of precipitation, and the significance of these correlations. Finally, in the third subsection, we identify the impact of potential moisture sources on the isotopic composition of precipitation.

3.1 Local Meteoric Water Line

The LMWL for the Treasure Valley of SW Idaho (Figure 8) has a slope of 7.10 (+/- 0.01) and a y-intercept of -6.3 (+/- 0.2, Equation 3). While the slope is similar to that of the GMWL (m = 8.13), the y-intercept of the LMWL is considerably different than the GMWL (b = +10.8).

$$\delta^2H = 7.10*\delta^{18}O - 6.3 \quad (3)$$

Timing of precipitation collection was categorized into dry-season (June 1st-September 30th) and wet-season (October 1st – May 31st), resulting in the LMWL comprising 36 dry season and 357 wet season samples. Deviation from the GMWL is a result of the semiarid climate of SW Idaho, and is especially pronounced during the dry season when secondary evaporation can be significant (Peng et al. 2007).

Fractionation processes result in a strong seasonal variance in the isotopic composition of precipitation, complicating the LMWL of the Treasure Valley (Figure 9). Linear regression of dry season precipitation results in a LMWL with slope 6.3 (+/- 0.01) and a y-intercept of -17.0 (+/- 0.2, Equation 4), while wet season precipitation results in a LMWL with slope 7.5 (+/- 0.01) and a y-intercept of -0.88 (+/- 0.2, Equation 5).

Dry Season: $\delta^2H = 6.3*\delta^{18}O - 17.0$ **(4)**

Wet Season: $\delta^2H = 7.5*\delta^{18}O - 0.88$ **(5)**

The signficant difference in the y-intercept (-16.12) is likely a result of increased secondary evaporation processes after precipitation exits a cloud during dry season events (Peng et al. 2007). The controlled evaporative enrichment experiment suggests it is highly unlikely the variation in the isotopic composition of precipitation during the dry season arose through a processes of enrichment after cessation of precipitation and before retrieval of samples. This supports the notion that the dry season slope and intercept of the LMWL are significantly different from the wet season and that the corresponding

values during the dry season arise from secondary evaporation during precipitation events.

We created a seasonally weighted LMWL (Figure 10) due to the seasonality of significant precipitation events. On average, 92% of the annual precipitation occurs during the wet season at the 3 collection sites in Dry Creek Experimental Watershed. Treating all events equal when the amount of summer precipitation is minimal, as was done in Figure 4, skews the linear regression towards the evaporatively enriched dry season samples. Therefore, we applied 92% weight to the wet season events and 8% weight to the dry season events. This method yields a LMWL with slope 7.4 (+/- 0.01) and a y-intercept of -2.17 (+/- 0.2, Equation 6), which is closer to the wet season LMWL (Equation 5) than the LMWL highlighted in Equation 3. We propose that this LMWL, weighted on a precipitation-mass basis, better represents the LMWL for this region and should be used when the stable isotopes of water are being used to constrain water mass fluxes, storages, and transit time in the region.

$$\delta^2H = 7.4*\delta^{18}O - 2.17 \quad (6)$$

3.2 Hydrometeorological Controls

Figure 11 shows the measured $\delta^{18}O$ of precipitation, plotted against the average temperature at the surface for the duration of individual events. A strong positive correlation exists between the two parameters ($r = 0.63$) that is statistically significant at $p < 0.05$. This reveals information regarding the connectivity between the isotopic

composition of precipitation and surface air temperature, and the linkage between surface temperature and the dew point temperature. The magnitude of equilibrium fractionation between vapor and liquid is a function of the temperature at the point of water vapor condensation and is thought to be one of the major controls on the isotopic composition of precipitation, along with moisture source history (Dansgaard 1964). Therefore, the strong correlation between surface temperature and the isotopic composition of precipitation suggests a relationship between surface air temperature and the temperature at which water vapor is condensing.

The correlation between surface temperature and the isotopic composition of precipitation is often more pronounced in the Rocky Mountain regions of the United States (Welker 2000). This is likely the result of moisture being predominantly from one source, the Pacific Ocean, while other regions of the United States receive moisture from several major sources (Gulf of Mexico, Pacific Ocean, Atlantic Ocean, coastal convection). Figure 12 also displays $\delta^{18}O$ of precipitation, plotted against the average surface temperature at each study site in DCEW. On visual inspection, little variability in the relationship between $\delta^{18}O$ and temperature exists between sites, with the most noticeable difference being a smaller temperature range at Lower Weather, which is the lowest elevation study site.

A moderate to strong negative correlation ($r = -0.57$) exists between the measured $\delta^{18}O$ of precipitation and the average relative humidity from individual events and is statistically significant at $p < 0.05$ (Figure 13). Five of the six events with the lowest average relative humidity occurred during the dry season (June through September), which is expected in a semiarid, mid-latitude climate. The five least humid dry season

precipitation events were also the most isotopically enriched. Relative humidity is related to the seasonality of events in this region since there are distinct wet and dry seasons. Secondary evaporation while precipitation is falling from the cloud base to the ground results in precipitation that is enriched isotopically relative to the original precipitation formed by condensed water vapor. The association between isotopically enriched precipitation and low humidity reflects an increased potential evaporation as precipitation transits from cloud base to the ground through a large driving vapor pressure deficit (Peng et al. 2007).

Little variability is seen among the three DCEW sample sites in the relationship between humidity and $\delta^{18}O$ (Figure 14). Interestingly, however, the three lowest humidity events occurred at Lower Deer Point and Treeline study sites, the two highest elevation sites in DCEW. The fact that there are no precipitation events associated with correspondingly low relative humidity at the Lower Weather site, the lowest elevation study site, likely reflects the scattered nature of summer convective precipitation and the increased secondary evaporation potential due to the greater distance between the cloud base and the ground.

The relationship between measured $\delta^{18}O$ of precipitation, precipitation amount, and storm intensity is shown in Figures 15-18. The $\delta^{18}O$ of precipitation and precipitation amount from individual events correlates moderately negatively ($r = -0.47$), as does the $\delta^{18}O$ of precipitation and storm intensity ($r = -0.36$). Both correlations are statistically significant at the 95% confidence interval. The Amount Effect, which is the isotopic depletion of precipitation with intense and continual precipitation events (Dansgaard 1964), potentially contributes to the correlation between $\delta^{18}O$ of precipitation and

precipitation amount. Higher frequency and longer duration precipitation events tend to be associated with increased relative humidity, which decreases potential evaporation and, therefore, suppresses kinetic fractionation.

However, the seasonality of larger volume events is also revealed in this correlation and is likely a greater control than the Amount Effect. Of the 25 largest precipitation events, 21 of these events occurred during the wet season (Oct – May) and the 9 largest precipitation events all occurred during the wet season. The wet season events, which are also often larger in magnitude in this region, undergo greater Rayleigh distillation, resulting in more isotopically depleted precipitation events. This also underscores that, from a watershed water balance perspective, these non-summer precipitation events are the most significant, further supporting our proposed seasonal-weighted LMWL above. The most important meteoric water from a hydrological perspective is non-summer precipitation at this location, with summer (dry season) precipitation events mostly amount limited.

There is no significant correlation between the temperature of the LCL for each event and the corresponding $\delta^{18}O$ of precipitation ($r = 0.13$, Figure 19). Air mass history and the temperature of water vapor condensation are thought to be the two major factors controlling the isotopic composition of precipitation (Dansgaard 1964). We only determined the temperature of the cloud base (i.e., where water vapor beings to condense to liquid water), rather than the average condensation temperature for precipitation events, which would likely be a better reflection of the rate of equilibrium fractionation. The lack of a correlation between $\delta^{18}O$ and the temperature at the LCL suggests that the parameter is a poor proxy for the rate of equilibrium fractionation.

The amount-weighted isotopic composition of precipitation, plotted against the elevation of the collection sites results in a very strong negative correlation ($r = -0.98$, $p < 0.02$, Figure 20). For every 100 m gained in elevation, the average $\delta^{18}O$ of precipitation decreases by 0.22 ‰. This is consistent with findings from other Altitude effect studies outlined by Ambach et al. (1968), with typical $\delta^{18}O$ decreases of 0.15 to 0.5 ‰ per 100 m, and reflects the direct connection between the isotopic composition of precipitation and the fractionation processes associated with orographic lift. In complex terrain, the isotopic composition of precipitation is highly variable at the event-scale, creating major complications for catchment transit time estimation studies. However, at climatological time scales, the variability conforms to the Altitude effect, providing some degree of predictability at seasonal to annual time-scales. In watersheds characterized by complex terrain, therefore, isotopic compositions can be distributed with knowledge of elevation and precipitation lapse rates over relevant time scales.

3.3 Moisture Sources

Using the NOAA HYSPLIT model, we were able to classify 4 predominant moisture sources for the 25 largest precipitation events in Dry Creek Experimental Watershed from May 2011 – May 2012. Event moisture tracked coastal over Oregon/Northern California for 12 events (Figure 21), while 8 events tracked over Southern California (Figure 22) and 3 events tracked over the Washington/Canadian coast line (Figure 23). Coastal sources from inland convection were associated with 2 summer events.

The average isotopic composition of all events from each moisture track location shows ^{18}O of precipitation is enriched from Washington/Canada sources compared to

Oregon/N. California and S. California (Figure 24). This was unexpected because fractionation during evaporation increases in colder regions as a result of greater difference in bonding energies, leaving the subsequent water vapor more depleted isotopically than water vapor from warm regions. However, the temperature gradients between potential moisture source locations and precipitation events may be more important than the moisture source locations themselves, since increased temperature gradients result in greater Rayleigh distillation.

We did not attempt to determine the location of ocean evaporation for the events analyzed, but instead located where moisture sources moved coastal for each event. The uneven distribution of moisture sources and the seasonality of events make comparative analyses problematic, requiring more analyses to draw meaningful conclusions. Additionally, the location an air parcel moves coastally does not necessarily equate with moisture source. Wind moves counterclockwise towards low pressure centers in the Northern Hemisphere. For instance, low pressure systems of sufficiently large size in the Gulf of Alaska off the coast of the Pacific Northwest can result in storms that move coastal over the Oregon Coast.

4. Conclusions

The LMWL of the greater-Boise area is considerably influenced by the semiarid climate of southwest Idaho, yielding a slope and y-intercept lower than the GMWL. Summer precipitation follows an evaporation enrichment line and is likely a result of the occurrence of significant secondary evaporation between the cloud base and the ground. Summer precipitation (dry season) events are typically smaller in volume than wet season events, with 8% of the total annual precipitation occurring between June 1st – Sept. 31st.

Therefore, we developed a seasonally weighted version of the LMWL to account for the large variation in precipitation arriving in the wet versus dry seasons. The seasonally weighted LMWL yields a slope of 7.4 and a y-intercept of -2.17, which we propose better represents the Treasure Valley LMWL than the non-seasonally weighted LMWL (m = 7.1, b = -6.3), which over-weights low-volume samples that have likely undergone secondary evaporation.

While our research and previous studies have discovered significant correlations between hydrometeorlogical variables and the isotopic composition of precipitation (Dansgaard 1964, Welker 2000), variations in the isotopic composition of precipitation cannot be explained by one variable. The variability is the result of dynamic physical processes that control and alter the isotope composition of precipitation (e.g., temperature, relative humidity, storm duration, precipitation amount, storm track, secondary evaporation, etc.). Additionally, the isotopic composition of precipitation is dependent on the sea surface temperature and the relative humidity at the moisture source location, along with the amount of rain-out along the storm track following a Rayleigh-type distillation process (Dansgaard 1964). Further work is needed to better constrain moisture sources and, thereby, improve predictability in the isotopic composition of precipitation.

Our research suggests the altitude effect in DCEW is significant, which is in agreement with previous studies (Poage and Chamberlain 2001, Dansgaard 1964). Since the isotopic composition of precipitation varies spatially, particularly in complex terrain, assuming homogeneity is not sufficient for isotope-based tracer studies. This finding has significant implications for estimating the distribution of transit times. When determining

the input function for transit time distribution estimation in catchments with complex terrain, the altitude effect suggests that elevation exerts a strong control on the isotopic composition of precipitation. However, this correlation is strongest only at seasonal to annual time-scales.

Additionally, orographic lift enhances the amount of precipitation at higher elevations in complex terrain. At the same time, the Altitude effect implies that, on average, precipitation is increasingly isotopically depleted at higher elevations. For event-scale determination of the isotopic input function to a watershed, therefore, we propose an approach that combines the relationship between the isotopic composition of precipitation with the relationship between precipitation volume and elevation to obtain a weighted-average isotopic composition input to the watershed. Over the long term, this method will more accurately represent the true spatial contribution of the isotopic composition of precipitation to the catchment, and may improve transit time distribution estimates. However, event-scale variations from the strong relationship between elevation and isotopic composition of precipitation could introduce large uncertainties into estimation of travel time distributions when a relatively small number of events are considered.

Appendix A

Table 1: Isotopic composition of 393 precipitation samples from various sites in the greater-Boise area.

Site	Collection Date	δ^2H ‰	$\delta^{18}O$ ‰
Bogus Ridge	1/20/2012	-161.99	-22.17
Bogus Ridge	1/24/2012	-104.47	-14.14
Bogus Ridge	1/27/2012	-127.29	-16.61
Bogus Ridge	2/2/2012	-146.64	-20.54
Bogus Ridge	2/15/2012	-144.53	-19.95
Bogus Ridge	2/15/2012	-114.10	-15.77
Bogus Ridge	3/16/2012	-124.86	-16.42
Bogus Ridge	3/17/2012	-116.57	-14.57
Bogus Ridge	3/19/2012	-129.14	-16.94
Bogus Ridge	3/21/2012	-135.86	-17.46
Boise State University	12/1/2010	-139.51	-18.61
Boise State University	12/7/2010	-171.22	-22.72
Boise State University	12/20/2010	-107.99	-14.43
Boise State University	12/27/2010	-144.41	-19.84
Boise State University	12/29/2010	-179.67	-22.93
Boise State University	1/17/2011	-119.56	-15.13
Boise State University	1/19/2011	-85.64	-11.78
Boise State University	1/25/2011	-83.87	-11.59
Boise State University	2/17/2011	-114.81	-15.63
Boise State University	3/7/2011	-143.37	-18.55
Boise State University	3/10/2011	-122.07	-14.27
Boise State University	3/17/2011	-106.33	-13.51
Boise State University	3/22/2011	-151.31	-20.39
Boise State University	3/24/2011	-87.75	-11.64
Boise State University	3/25/2011	-150.92	-20.11
Boise State University	3/29/2011	-131.73	-17.63
Boise State University	3/30/2011	-122.17	-15.44
Boise State University	4/2/2011	-86.96	-10.86
Boise State University	4/21/2011	-125.36	-16.81
Boise State University	4/25/2011	-93.92	-12.02
Boise State University	4/28/2011	-97.83	-13.04
Boise State University	5/7/2011	-92.92	-10.93
Boise State University	5/8/2011	-117.85	-15.38
Boise State University	5/16/2011	-114.93	-15.06
Boise State University	5/26/2011	-72.99	-10.74

Boise State University	6/3/2011	-54.74	-4.73
Boise State University	6/30/2011	-75.32	-7.03
Boise State University	7/14/2011	-74.15	-6.81
Boise State University	9/16/2011	-25.13	-2.49
Boise State University	10/6/2011	-94.21	-12.11
Boise State University	10/6/2011	-106.99	-13.99
Boise State University	10/11/2011	-140.67	-17.60
Boise State University	10/11/2011	-143.68	-18.46
Boise State University	10/17/2011	-98.82	-12.99
Capital High School	10/5/2011	-56.54	-8.14
Capital High School	11/18/2011	-80.77	-10.77
Capital High School	1/18/2012	-135.91	-18.03
Capital High School	1/19/2012	-130.97	-16.19
Capital High School	1/24/2012	-123.73	-16.63
Capital High School	1/26/2012	-94.79	-12.10
Crimson Point Elementary	11/18/2011	-78.83	-10.54
Crimson Point Elementary	1/18/2012	-197.06	-25.49
Crimson Point Elementary	1/18/2012	-204.24	-26.48
Da Vinci Charter	2/2/2012	-98.69	-11.99
Da Vinci Charter	3/19/2012	-120.83	-15.07
Euclid	9/15/2011	-20.98	-1.14
Euclid	10/5/2011	-77.66	-9.97
Euclid	10/11/2011	-148.00	-18.70
Euclid	10/17/2011	-99.10	-13.03
Euclid	1/19/2012	-152.71	-20.78
Euclid	1/26/2012	-115.69	-15.89
Euclid	3/17/2012	-108.10	-13.61
Euclid	3/19/2012	-115.59	-14.73
Euclid	4/26/2012	-112.20	-14.52
Euclid	5/1/2012	-59.15	-6.53
Lower Deer Point	10/14/2009	-131.86	-15.51
Lower Deer Point	10/14/2009	-169.81	-22.20
Lower Deer Point	10/15/2009	-79.78	-9.97
Lower Deer Point	10/15/2009	-63.46	-9.41
Lower Deer Point	10/15/2009	-54.69	-7.64
Lower Deer Point	10/19/2009	-88.57	-12.64
Lower Deer Point	10/24/2009	-110.78	-15.09
Lower Deer Point	10/30/2009	-88.63	-12.83
Lower Deer Point	11/7/2009	-71.76	-10.56

Lower Deer Point	11/13/2009	-150.39	-19.06
Lower Deer Point	1/13/2010	-84.22	-11.37
Lower Deer Point	1/20/2010	-131.73	-15.63
Lower Deer Point	1/20/2010	-136.24	-17.27
Lower Deer Point	3/29/2010	-118.34	-15.84
Lower Deer Point	4/2/2010	-108.70	-14.57
Lower Deer Point	4/15/2010	-125.44	-16.64
Lower Deer Point	4/20/2010	-114.25	-15.17
Lower Deer Point	4/21/2010	-110.42	-15.23
Lower Deer Point	4/24/2010	-99.68	-12.43
Lower Deer Point	5/7/2010	-101.36	-13.34
Lower Deer Point	5/12/2010	-106.79	-14.07
Lower Deer Point	5/19/2010	-103.61	-14.79
Lower Deer Point	5/25/2010	-104.54	-14.23
Lower Deer Point	5/28/2010	-100.80	-14.14
Lower Deer Point	6/5/2010	-113.98	-15.20
Lower Deer Point	6/7/2010	-110.87	-14.41
Lower Deer Point	6/11/2010	-61.63	-8.36
Lower Deer Point	6/21/2010	-71.25	-9.80
Lower Deer Point	10/25/2010	-134.04	-18.47
Lower Deer Point	10/27/2010	-79.52	-12.34
Lower Deer Point	11/1/2010	-94.02	-13.84
Lower Deer Point	11/8/2010	-126.88	-18.55
Lower Deer Point	11/11/2010	-104.91	-15.20
Lower Deer Point	11/15/2010	-98.53	-13.64
Lower Deer Point	12/7/2010	-130.12	-16.84
Lower Deer Point	1/17/2011	-148.73	-19.91
Lower Deer Point	5/7/2011	-130.28	-17.78
Lower Deer Point	5/16/2011	-129.08	-17.58
Lower Deer Point	5/19/2011	-112.96	-15.15
Lower Deer Point	5/26/2011	-83.75	-12.47
Lower Deer Point	5/27/2011	-115.98	-16.06
Lower Deer Point	6/7/2011	-100.52	-13.74
Lower Deer Point	6/9/2011	-103.45	-14.71
Lower Deer Point	6/29/2011	-84.00	-9.91
Lower Deer Point	6/30/2011	-99.43	-12.31
Lower Deer Point	9/11/2011	-70.64	-10.18
Lower Deer Point	9/15/2011	-39.23	-3.19
Lower Deer Point	9/16/2011	-52.59	-7.71
Lower Deer Point	10/5/2011	-93.89	-13.54
Lower Deer Point	10/7/2011	-167.90	-22.76

Lower Deer Point	10/17/2011	-119.80	-16.48
Lower Deer Point	11/5/2011	-112.21	-16.53
Lower Deer Point	11/13/2011	-85.62	-13.04
Lower Deer Point	11/22/2011	-167.41	-23.48
Lower Deer Point	12/27/2011	-101.51	-13.63
Lower Deer Point	12/31/2011	-100.36	-13.87
Lower Deer Point	1/20/2012	-157.65	-21.76
Lower Deer Point	1/22/2012	-100.55	-14.33
Lower Deer Point	1/24/2012	-158.73	-21.37
Lower Deer Point	1/27/2012	-104.95	-12.95
Lower Deer Point	2/3/2012	-135.99	-18.44
Lower Deer Point	2/15/2012	-133.19	-18.27
Lower Deer Point	3/18/2012	-130.16	-17.56
Lower Deer Point	3/19/2012	-124.73	-16.08
Lower Deer Point	3/21/2012	-122.04	-15.74
Lower Deer Point	3/27/2012	-96.29	-13.33
Lower Deer Point	3/28/2012	-113.09	-15.05
Lower Deer Point	4/19/2012	-105.75	-14.54
Lower Deer Point	4/26/2012	-121.82	-16.58
Lower Deer Point	4/27/2012	-110.39	-12.88
Lower Deer Point	5/1/2012	-75.86	-11.09
Lower Deer Point	5/5/2012	-92.18	-13.09
Lower Deer Point	5/23/2012	-66.86	-9.86
Lower Weather	10/6/2009	-137.96	-19.20
Lower Weather	10/19/2009	-71.19	-9.59
Lower Weather	10/19/2009	-70.80	-9.69
Lower Weather	10/24/2009	-83.97	-10.63
Lower Weather	10/24/2009	-85.12	-10.81
Lower Weather	10/30/2009	-93.39	-12.69
Lower Weather	11/7/2009	-53.15	-7.15
Lower Weather	11/13/2009	-140.93	-18.66
Lower Weather	11/13/2009	-140.82	-18.65
Lower Weather	1/7/2010	-112.83	-15.65
Lower Weather	1/25/2010	-140.90	-17.87
Lower Weather	1/27/2010	-133.85	-18.10
Lower Weather	2/1/2010	-179.15	-23.77
Lower Weather	2/10/2010	-127.65	-15.35
Lower Weather	2/17/2010	-75.34	-9.42
Lower Weather	2/24/2010	-164.83	-20.85
Lower Weather	2/28/2010	-110.39	-12.95
Lower Weather	3/5/2010	-100.24	-12.65

Lower Weather	3/9/2010	-96.81	-12.79
Lower Weather	3/15/2010	-118.51	-14.75
Lower Weather	3/26/2010	-84.71	-11.51
Lower Weather	4/2/2010	-80.13	-9.93
Lower Weather	4/3/2010	-125.32	-15.95
Lower Weather	4/13/2010	-98.57	-12.35
Lower Weather	4/21/2010	-75.81	-10.54
Lower Weather	4/30/2010	-114.87	-14.96
Lower Weather	5/7/2010	-80.88	-10.71
Lower Weather	5/12/2010	-102.44	-13.79
Lower Weather	5/19/2010	-72.61	-10.22
Lower Weather	5/24/2010	-117.97	-16.04
Lower Weather	5/30/2010	-91.87	-12.27
Lower Weather	6/1/2010	-70.63	-6.94
Lower Weather	6/5/2010	-100.12	-12.39
Lower Weather	6/11/2010	-43.32	-4.75
Lower Weather	6/21/2010	-49.32	-5.72
Lower Weather	10/25/2010	-127.30	-16.33
Lower Weather	10/27/2010	-72.94	-11.43
Lower Weather	11/1/2010	-74.22	-10.22
Lower Weather	11/8/2010	-109.63	-15.45
Lower Weather	11/15/2010	-83.27	-11.35
Lower Weather	12/7/2010	-144.44	-19.59
Lower Weather	12/7/2010	-144.93	-19.80
Lower Weather	12/13/2010	-70.60	-10.24
Lower Weather	12/15/2010	-129.92	-17.20
Lower Weather	12/27/2010	-133.90	-17.96
Lower Weather	12/29/2010	-177.12	-23.35
Lower Weather	1/17/2011	-123.45	-16.19
Lower Weather	1/25/2011	-91.66	-12.80
Lower Weather	3/8/2011	-149.49	-19.30
Lower Weather	3/11/2011	-105.21	-13.89
Lower Weather	3/14/2011	-87.44	-10.61
Lower Weather	3/17/2011	-111.05	-14.41
Lower Weather	3/22/2011	-134.18	-18.17
Lower Weather	3/25/2011	-120.80	-16.53
Lower Weather	3/31/2011	-130.90	-17.19
Lower Weather	4/2/2011	-92.92	-12.85
Lower Weather	4/5/2011	-72.83	-9.86
Lower Weather	4/17/2011	-139.78	-18.84
Lower Weather	4/22/2011	-105.00	-13.25

Lower Weather	4/26/2011	-98.00	-13.25
Lower Weather	4/30/2011	-95.71	-12.79
Lower Weather	5/7/2011	-102.03	-12.75
Lower Weather	5/8/2011	-129.92	-17.19
Lower Weather	5/16/2011	-124.06	-16.73
Lower Weather	5/19/2011	-94.55	-12.79
Lower Weather	5/27/2011	-94.26	-12.72
Lower Weather	6/2/2011	-121.64	-16.51
Lower Weather	6/7/2011	-80.33	-11.14
Lower Weather	6/9/2011	-86.11	-12.09
Lower Weather	6/29/2011	-72.75	-7.23
Lower Weather	6/30/2011	-80.71	-7.52
Lower Weather	9/16/2011	-39.06	-5.04
Lower Weather	10/5/2011	-82.01	-11.21
Lower Weather	10/7/2011	-152.86	-20.46
Lower Weather	10/11/2011	-142.84	-18.32
Lower Weather	10/17/2011	-110.68	-14.79
Lower Weather	11/5/2011	-109.63	-15.77
Lower Weather	11/22/2011	-126.83	-17.34
Lower Weather	12/29/2011	-107.10	-13.51
Lower Weather	12/31/2011	-84.29	-11.25
Lower Weather	1/20/2012	-148.88	-20.26
Lower Weather	1/24/2012	-127.75	-16.59
Lower Weather	1/27/2012	-98.91	-12.08
Lower Weather	2/2/2012	-147.88	-20.16
Lower Weather	2/15/2012	-103.93	-13.98
Lower Weather	2/27/2012	-93.24	-11.83
Lower Weather	3/16/2012	-112.53	-14.88
Lower Weather	3/18/2012	-119.65	-15.35
Lower Weather	3/19/2012	-125.82	-16.58
Lower Weather	3/21/2012	-118.51	-15.00
Lower Weather	3/26/2012	-84.20	-12.35
Lower Weather	3/28/2012	-113.94	-15.27
Lower Weather	4/19/2012	-83.53	-10.24
Lower Weather	4/26/2012	-117.88	-15.34
Lower Weather	4/27/2012	-116.91	-15.37
Lower Weather	5/1/2012	-62.70	-7.50
Lower Weather	5/5/2012	-93.44	-12.75
Lower Weather	5/23/2012	-60.59	-7.86
Mountain View High School	10/12/2011	-99.45	-12.99

Mountain View High School	10/17/2011	-100.75	-13.27
Mountain View High School	11/5/2011	-105.76	-14.56
Mountain View High School	1/18/2012	-118.29	-14.78
Mountain View High School	1/18/2012	-210.55	-27.27
Mountain View High School	1/20/2012	-145.77	-18.58
Mountain View High School	2/1/2012	-112.29	-14.49
Mountain View High School	2/25/2012	-94.59	-12.70
Mountain View High School	3/16/2012	-103.61	-12.44
Taft Elementary	10/5/2011	-119.85	-15.31
Taft Elementary	10/11/2011	-148.70	-18.49
Taft Elementary	1/9/2012	-132.58	-16.47
Taft Elementary	1/18/2012	-182.10	-23.42
Taft Elementary	1/19/2012	-132.65	-16.90
Taft Elementary	1/23/2012	-129.14	-17.11
Taft Elementary	1/26/2012	-114.54	-14.75
Taft Elementary	2/1/2012	-93.20	-11.82
Taft Elementary	3/15/2012	-112.91	-13.66
Taft Elementary	3/21/2012	-110.87	-13.85
Taft Elementary	4/16/2012	-52.54	-6.13
Taft Elementary	4/17/2012	-77.13	-9.53
Taft Elementary	4/19/2012	-99.73	-11.98
Taft Elementary	4/27/2012	-122.40	-16.10
Taft Elementary	4/27/2012	-115.08	-14.84
Taft Elementary	4/30/2012	-64.33	-7.06
Taft Elementary	5/3/2012	-72.05	-7.91
Taft Elementary	5/4/2012	-98.99	-13.40
Treeline	10/6/2009	-153.53	-21.27
Treeline	10/14/2009	-144.21	-18.35
Treeline	10/15/2009	-58.80	-8.64
Treeline	10/19/2009	-84.25	-12.38
Treeline	10/24/2009	-105.49	-14.32
Treeline	10/30/2009	-90.29	-12.75
Treeline	11/7/2009	-66.66	-10.15
Treeline	11/13/2009	-149.07	-19.81
Treeline	1/20/2010	-128.18	-16.56

Treeline	1/25/2010	-150.96	-19.74
Treeline	1/27/2010	-151.14	-19.94
Treeline	1/30/2010	-149.72	-19.49
Treeline	2/10/2010	-147.14	-19.07
Treeline	2/17/2010	-135.56	-17.26
Treeline	3/5/2010	-140.51	-18.14
Treeline	3/9/2010	-134.86	-17.56
Treeline	3/12/2010	-121.95	-15.72
Treeline	3/26/2010	-63.32	-7.82
Treeline	3/29/2010	-102.06	-13.27
Treeline	4/2/2010	-75.07	-10.13
Treeline	4/7/2010	-100.01	-12.89
Treeline	4/13/2010	-107.13	-13.81
Treeline	4/14/2010	-109.23	-14.24
Treeline	4/21/2010	-91.98	-12.59
Treeline	4/24/2010	-84.54	-11.06
Treeline	4/24/2010	-84.05	-11.09
Treeline	4/30/2010	-107.65	-13.85
Treeline	5/7/2010	-110.79	-15.48
Treeline	5/12/2010	-109.57	-15.50
Treeline	5/19/2010	-96.41	-13.25
Treeline	5/24/2010	-104.49	-14.64
Treeline	5/28/2010	-96.57	-13.40
Treeline	5/30/2010	-106.00	-14.45
Treeline	6/1/2010	-84.04	-10.50
Treeline	6/7/2010	-108.24	-13.69
Treeline	6/11/2010	-50.36	-6.43
Treeline	6/21/2010	-68.52	-9.61
Treeline	10/25/2010	-130.23	-17.48
Treeline	10/27/2010	-71.62	-11.79
Treeline	11/1/2010	-86.33	-12.58
Treeline	11/8/2010	-123.23	-17.59
Treeline	11/11/2010	-95.71	-13.97
Treeline	11/15/2010	-95.66	-13.10
Treeline	12/7/2010	-139.72	-19.34
Treeline	12/9/2010	-123.57	-16.85
Treeline	12/9/2010	-147.10	-20.60
Treeline	12/13/2010	-85.83	-12.44
Treeline	12/13/2010	-126.81	-17.85
Treeline	12/15/2010	-139.07	-19.26
Treeline	12/15/2010	-140.31	-19.15

Treeline	12/16/2010	-133.99	-18.13
Treeline	12/27/2010	-148.37	-19.72
Treeline	1/17/2011	-131.84	-17.99
Treeline	1/17/2011	-150.31	-20.20
Treeline	1/20/2011	-108.85	-15.01
Treeline	1/20/2011	-142.84	-19.07
Treeline	1/28/2011	-106.81	-14.82
Treeline	1/28/2011	-117.58	-14.66
Treeline	3/3/2011	-120.03	-15.63
Treeline	3/8/2011	-118.47	-15.81
Treeline	3/11/2011	-115.21	-15.10
Treeline	3/14/2011	-96.02	-13.04
Treeline	3/14/2011	-113.29	-15.09
Treeline	3/18/2011	-118.22	-16.03
Treeline	3/18/2011	-103.48	-14.28
Treeline	3/22/2011	-127.94	-17.13
Treeline	3/22/2011	-129.47	-17.22
Treeline	3/25/2011	-110.44	-15.64
Treeline	3/31/2011	-138.09	-18.18
Treeline	4/5/2011	-87.93	-12.73
Treeline	4/17/2011	-153.13	-21.14
Treeline	4/22/2011	-121.42	-15.77
Treeline	4/23/2011	-123.92	-16.63
Treeline	4/27/2011	-97.69	-13.78
Treeline	4/30/2011	-110.82	-14.82
Treeline	5/7/2011	-115.87	-15.16
Treeline	5/8/2011	-145.33	-19.78
Treeline	5/16/2011	-130.25	-17.52
Treeline	5/19/2011	-102.32	-13.66
Treeline	5/26/2011	-103.36	-14.79
Treeline	5/27/2011	-106.05	-14.69
Treeline	6/7/2011	-97.07	-13.46
Treeline	6/9/2011	-101.57	-14.57
Treeline	6/29/2011	-70.04	-7.41
Treeline	6/30/2011	-98.41	-11.59
Treeline	9/11/2011	-49.55	-6.37
Treeline	9/16/2011	-50.01	-7.07
Treeline	10/5/2011	-90.35	-12.50
Treeline	10/7/2011	-168.45	-22.60
Treeline	10/11/2011	-148.06	-19.60
Treeline	10/17/2011	-118.70	-16.34

Treeline	11/5/2011	-119.80	-15.98
Treeline	11/13/2011	-90.84	-13.99
Treeline	11/22/2011	-154.88	-21.78
Treeline	12/29/2011	-117.55	-15.73
Treeline	1/20/2012	-166.60	-22.57
Treeline	1/24/2012	-112.34	-15.87
Treeline	1/27/2012	-114.21	-14.99
Treeline	2/15/2012	-129.26	-17.70
Treeline	2/27/2012	-92.72	-12.69
Treeline	3/16/2012	-113.38	-15.55
Treeline	3/18/2012	-123.60	-16.27
Treeline	3/19/2012	-128.51	-16.10
Treeline	3/21/2012	-127.57	-16.82
Treeline	3/21/2012	-125.86	-16.42
Treeline	3/27/2012	-89.13	-12.89
Treeline	3/27/2012	-93.26	-13.27
Treeline	3/28/2012	-121.26	-15.89
Treeline	4/19/2012	-99.01	-13.60
Treeline	4/26/2012	-141.65	-19.15
Treeline	4/27/2012	-121.38	-16.53
Treeline	5/1/2012	-75.04	-10.38
Treeline	5/5/2012	-91.21	-12.56
Treeline	5/23/2012	-68.35	-9.78
Washington Elementary	11/18/2011	-76.32	-9.35
Washington Elementary	11/22/2011	-97.99	-12.68
Washington Elementary	12/28/2011	-111.00	-13.46
Washington Elementary	12/30/2011	-56.60	-6.46
Washington Elementary	1/18/2012	-184.08	-23.99
Washington Elementary	1/20/2012	-157.24	-19.91
Washington Elementary	1/22/2012	-133.75	-16.76
Washington Elementary	1/24/2012	-113.13	-15.02
Washington Elementary	1/30/2012	-94.42	-11.65
Washington Elementary	2/21/2012	-102.79	-13.32

Washington Elementary	3/6/2012	-111.08	-14.68
Washington Elementary	3/14/2012	-123.41	-15.78
Washington Elementary	3/19/2012	-113.26	-14.55
Washington Elementary	4/15/2012	-122.18	-15.73
Washington Elementary	4/17/2012	-93.90	-11.99
Washington Elementary	4/27/2012	-145.22	-18.86

Table 2: Average isotopic composition of precipitation from all sites.

Site	Average δ^2H ‰	Average $\delta^{18}O$ ‰	# of samples (n)	Elevation (m)
Bogus Ridge (only snow)	-130.54	-17.46	34	2114
Lower Deer Point	-107.55	-14.56	73	1850
Treeline	-112.43	-15.19	114	1610
Lower Weather	-105.56	-13.88	98	1151
Boise State University	-111.14	-14.27	34	823
Euclid	-100.92	-12.89	10	820
Capital High School	-103.79	-13.64	6	814
Crimson Point Elementary	-160.04	-20.83	3	792
Da Vinci Charter	-109.76	-13.53	2	804
Mountain View	-121.23	-15.68	9	762
Washington Elementary	-114.77	-14.64	16	829
Taft Elementary	-108.60	-13.66	17	830

Table 3: Seasonal Variations of greater-Boise LMWL.

Dataset	Slope (m)	Y-Intercept (b)	Correlation Coefficient (r^2)	# of Samples (n)
Winter Precipitation (Oct. – May)	7.5	-0.88	0.96	357
Summer Precipitation (June – Sep.)	6.3	-17.0	0.90	36
All Precipitation	7.1	-6.3	0.96	393

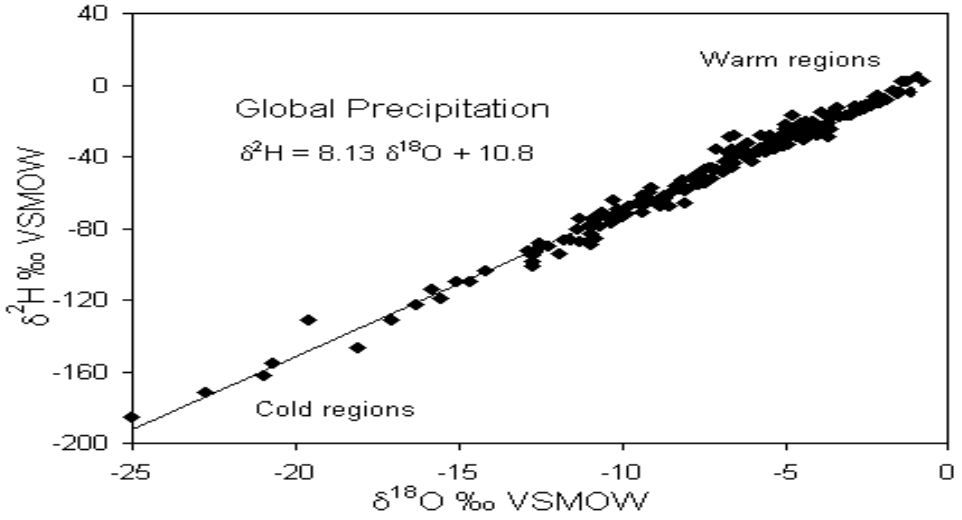

Figure 1: The Global Meteoric Water Line, as refined by Rozanski et al. (1992)

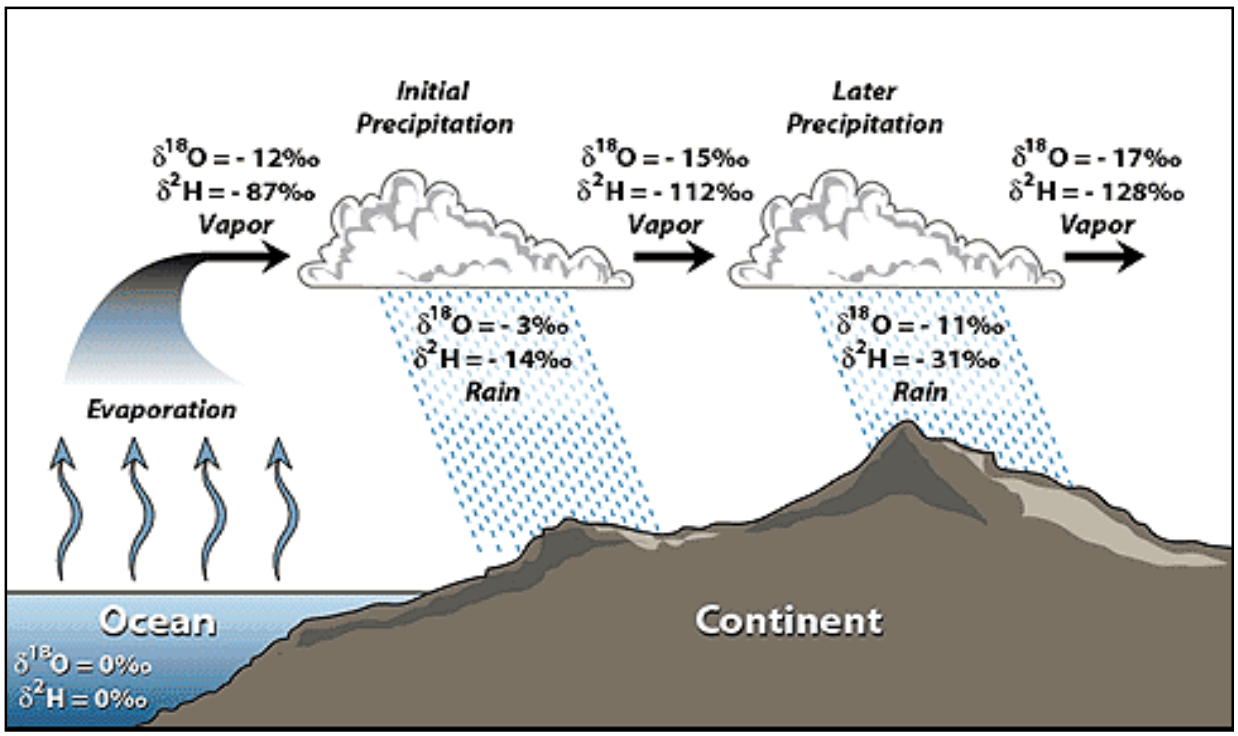

Figure 2: The Continental effect: Precipitation becomes more isotopically depleted the farther away air masses are from the original moisture source (Coplen et al. 2000, Hoefs 2009).

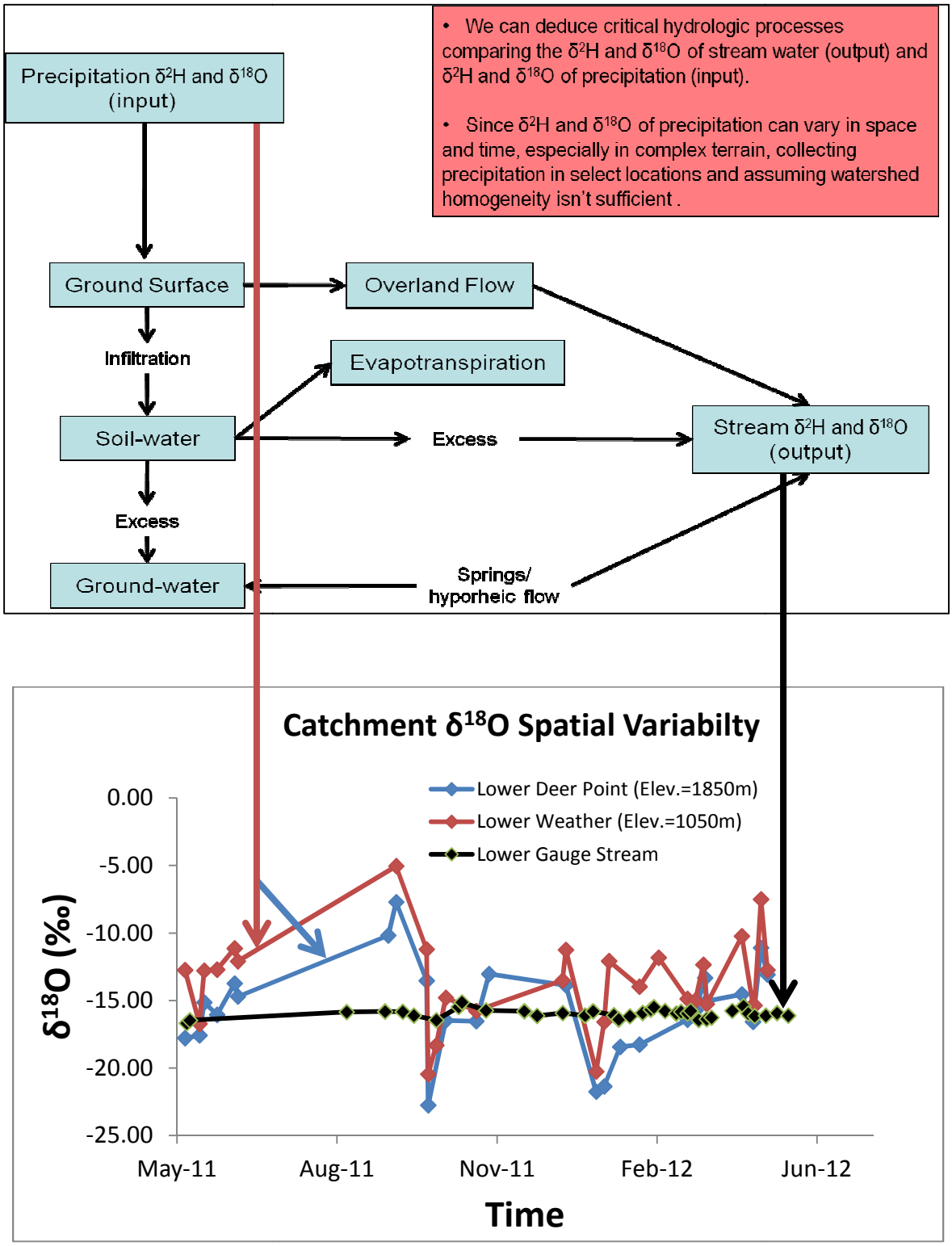

Figure 3: Conceptual model depicting the problems with transit time estimation using stable isotope composition of precipitation as environmental tracers.

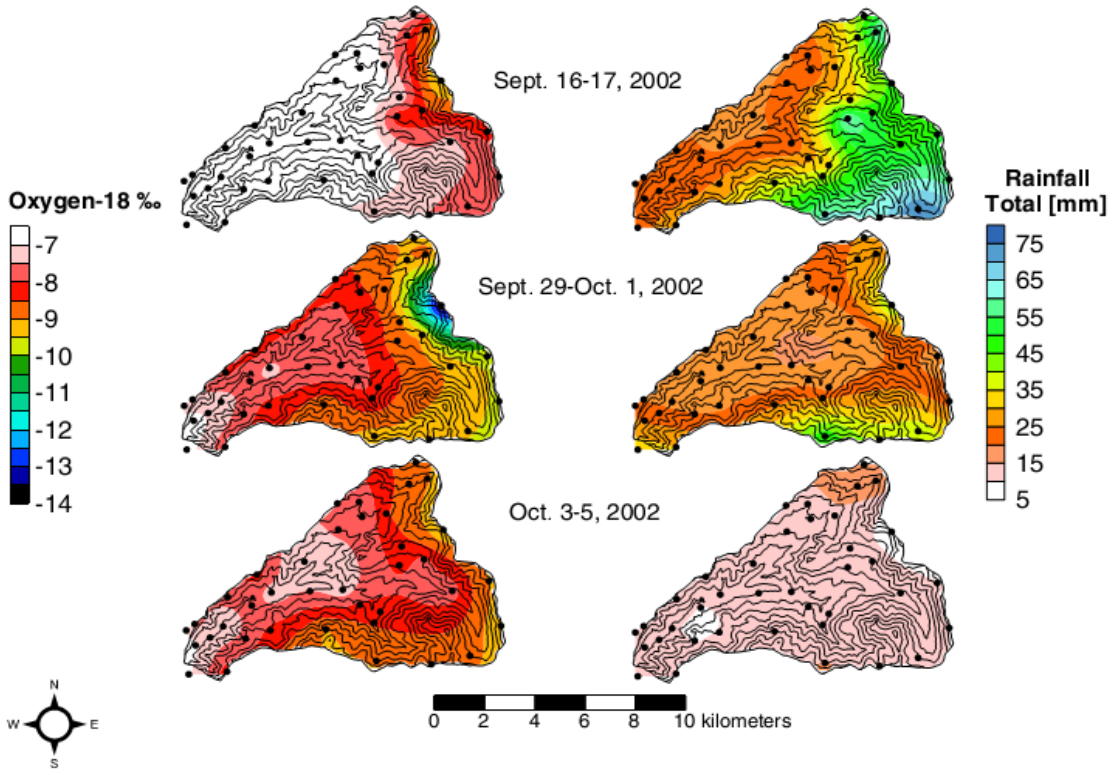

Figure 4: Variability in isotopic composition of precipitation in the Lookout Creek Watershed within western Oregon (McGuire & McDonnell 2006).

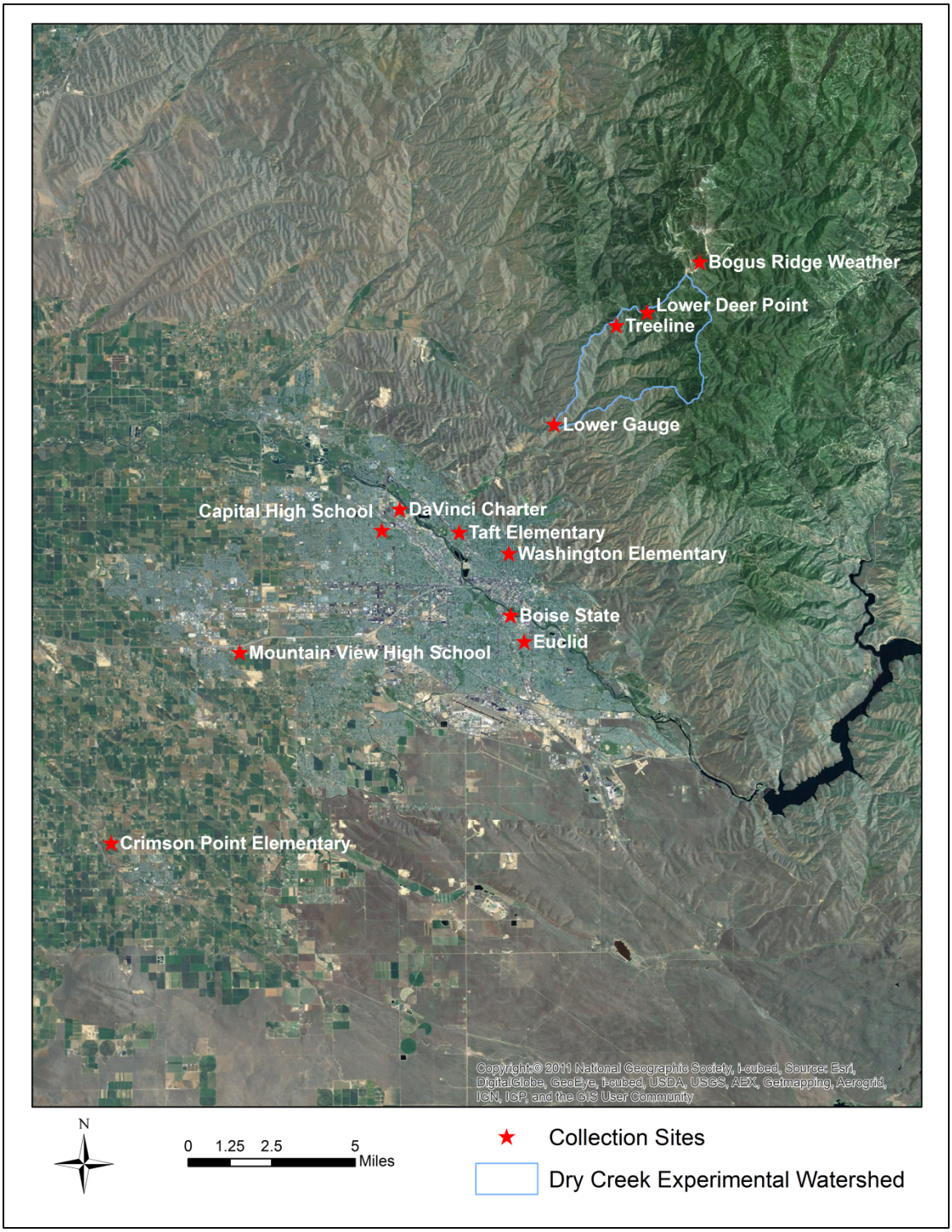

Figure 5: Greater-Boise precipitation collection sites comprising the LMWL.

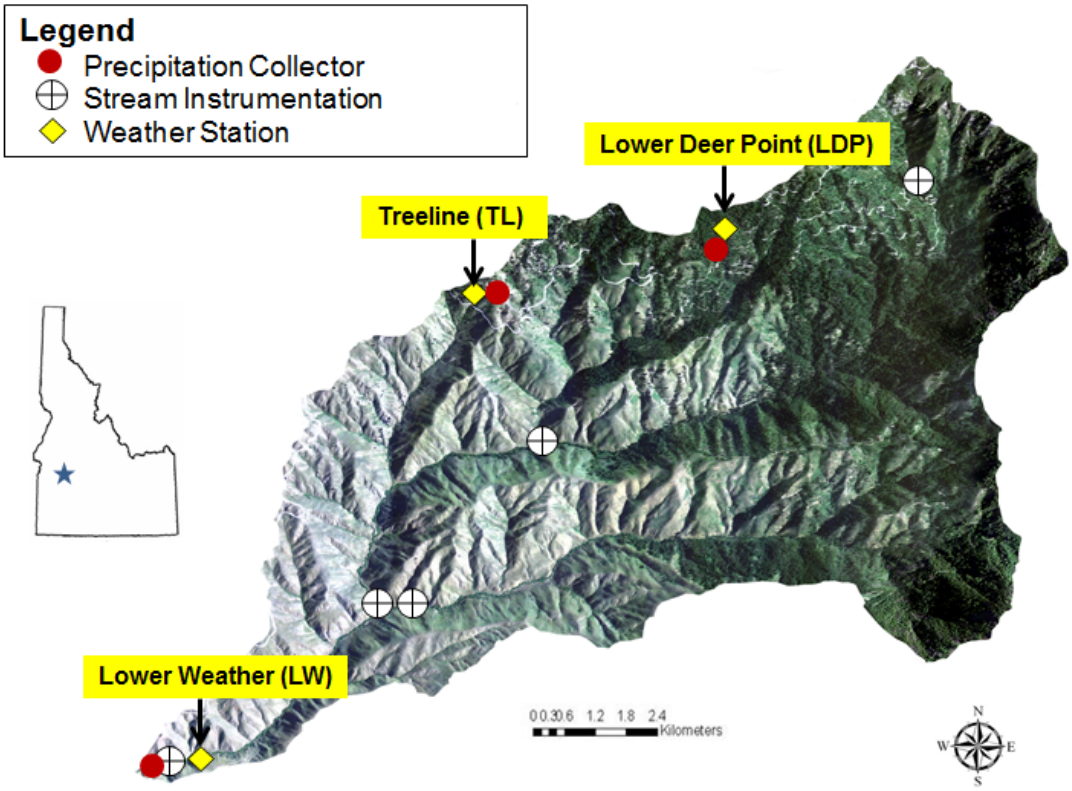

Figure 6: Dry Creek Experimental Watershed near Boise, ID.

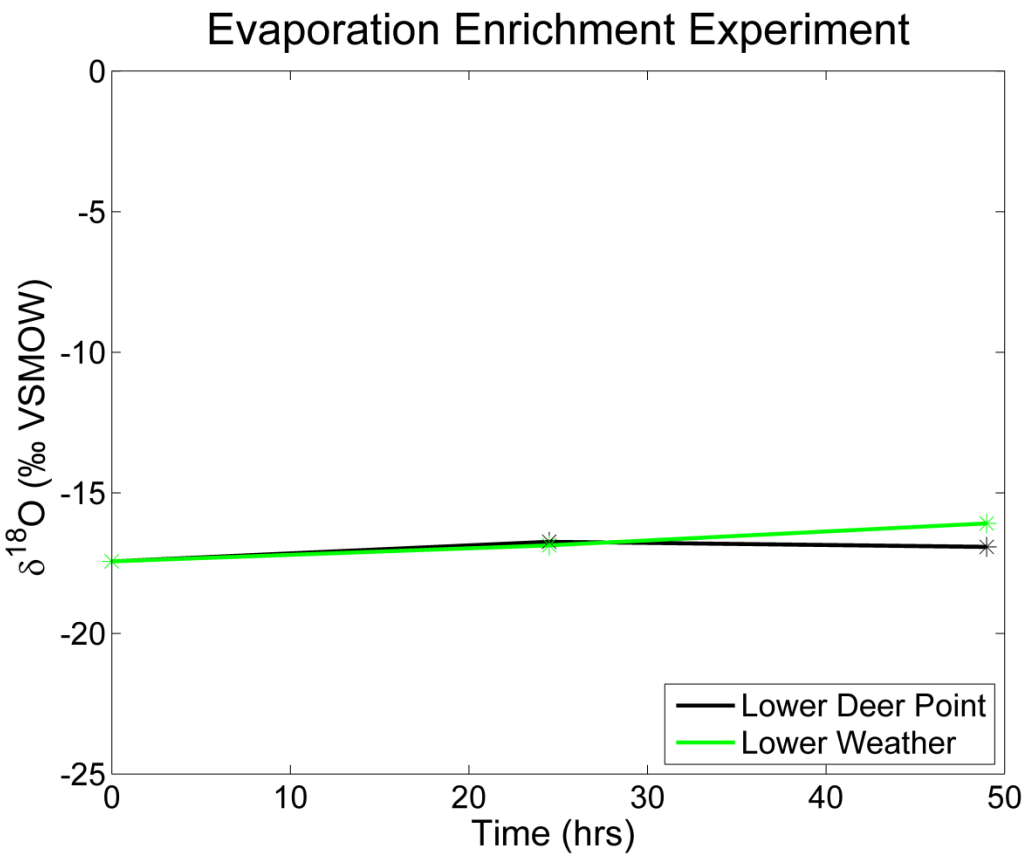

Figure 7: Evaporation enrichment experiment at 2 study sites in DCEW, performed from July 25-27th 2012. The $\delta^{18}O$ composition of the sample was enriched by less than 0.7 per mil after 50 hours. Maximum temperature at Lower Weather exceeded 90°F each day, and exceeded 80°F each day at Lower Deer Point

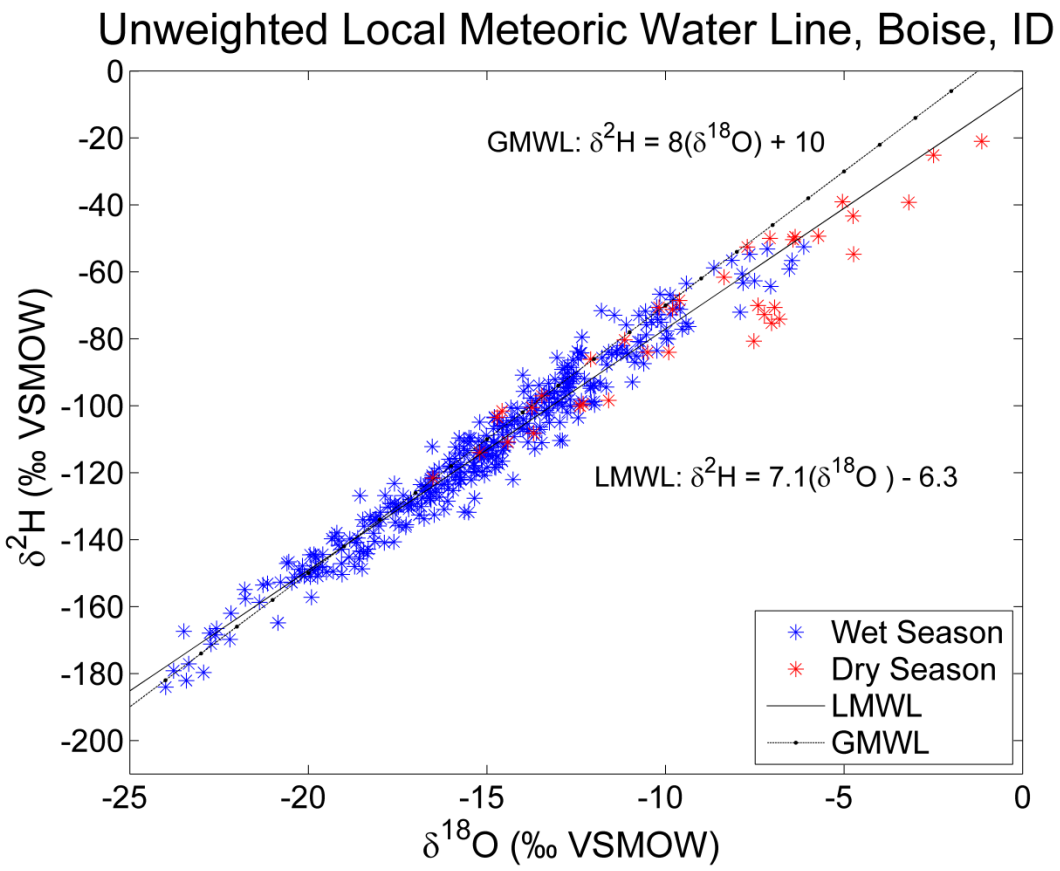

Figure 8: Local Meteoric Water Line for the Greater-Boise Area, events have equal weight.

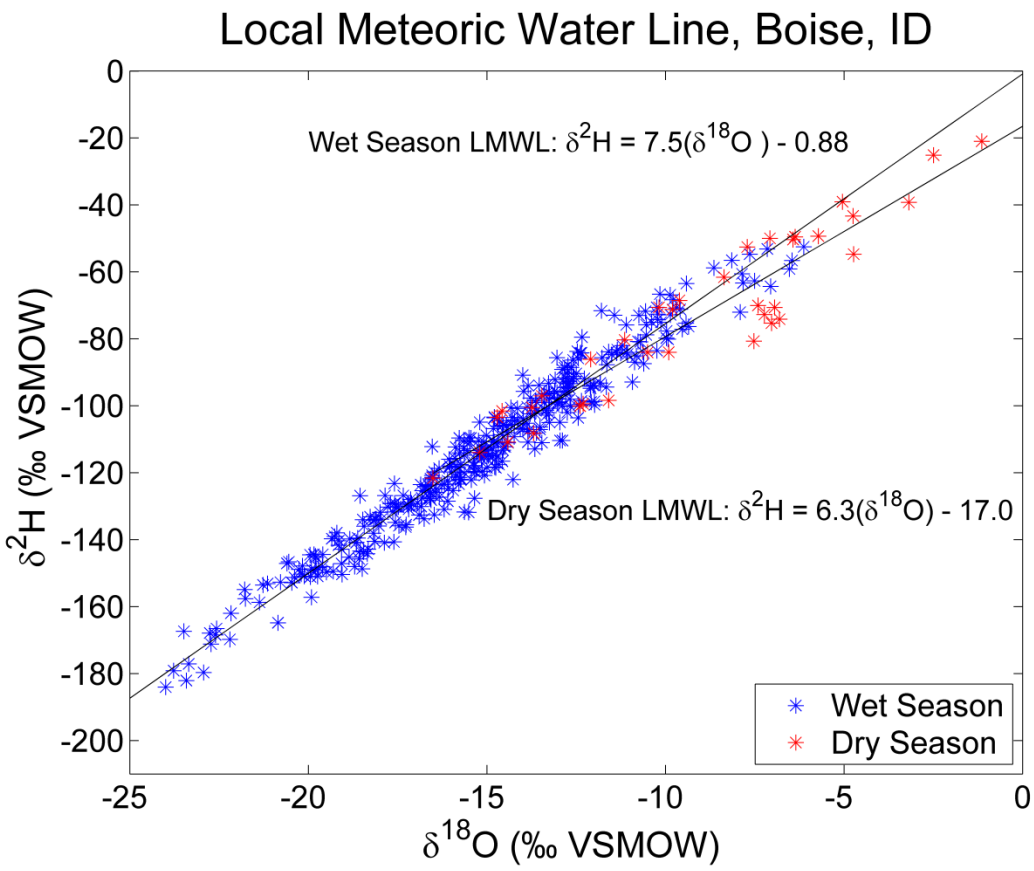

Figure 9: Variations in the LMWL depending on seasonality of precipitation. Dry Season (June – Sept) events follow an evaporation enrichment line.

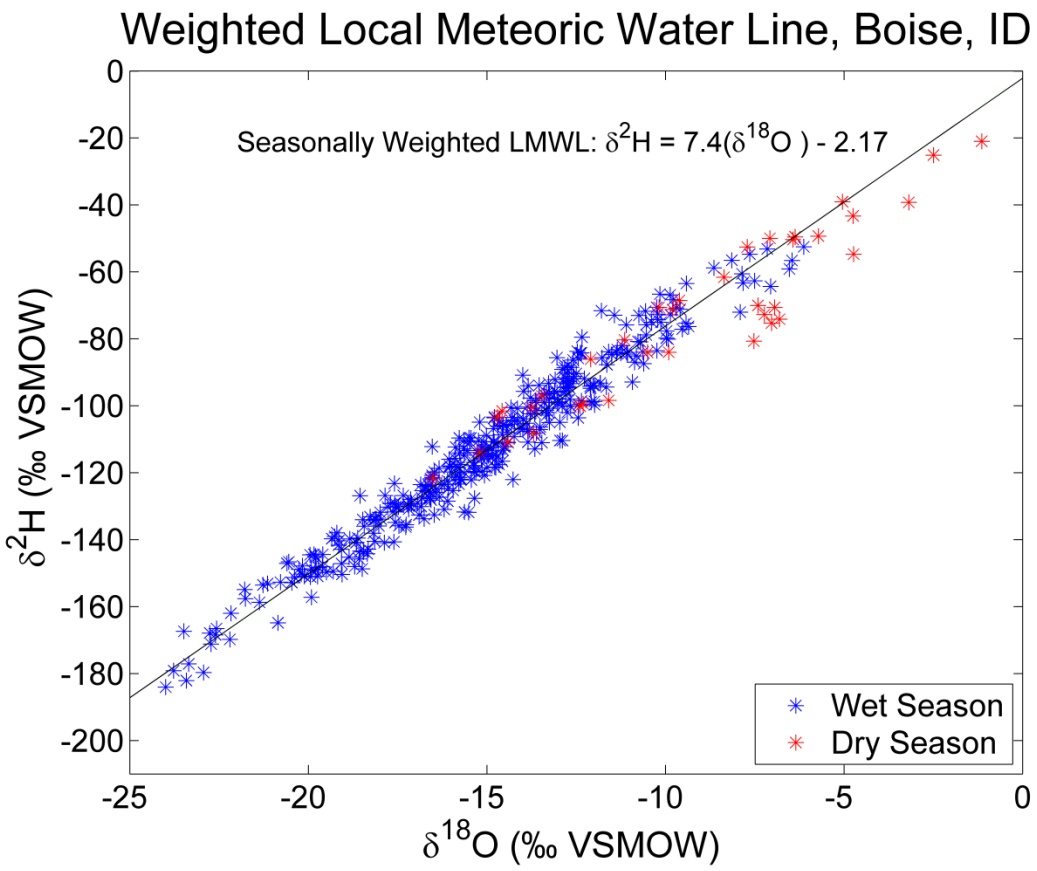

Figure 10: Seasonally weighted local meteoric water line based on occurrence of total annual precipitation percentages during dry season vs. wet season.

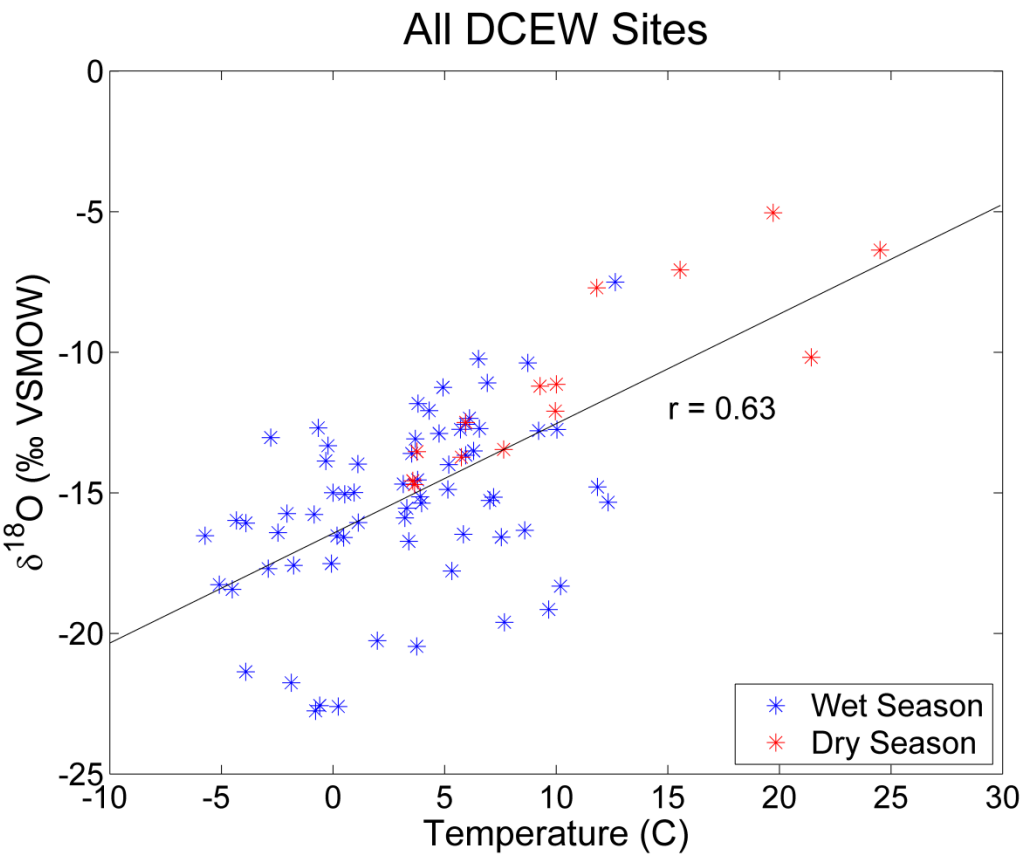

Figure 11: Relationship between $\delta^{18}O$ of precipitation and average surface temperature (C) for each precipitation event.

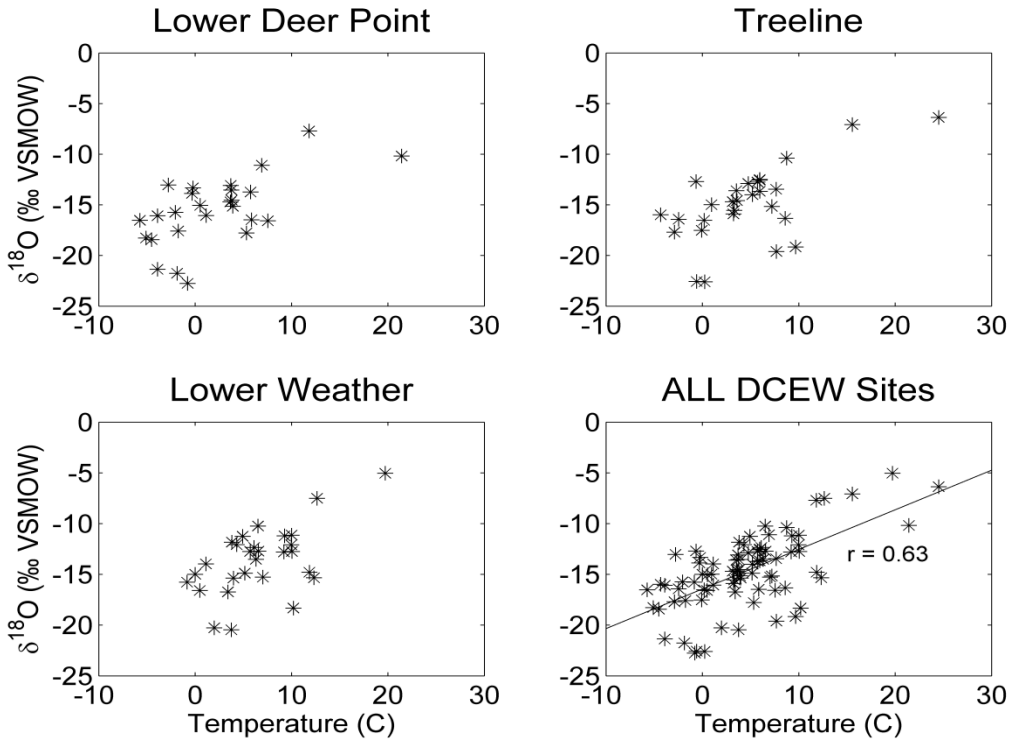

Figure 12: Relationship between $\delta^{18}O$ of precipitation and average surface temperature for each precipitation event at each collection site.

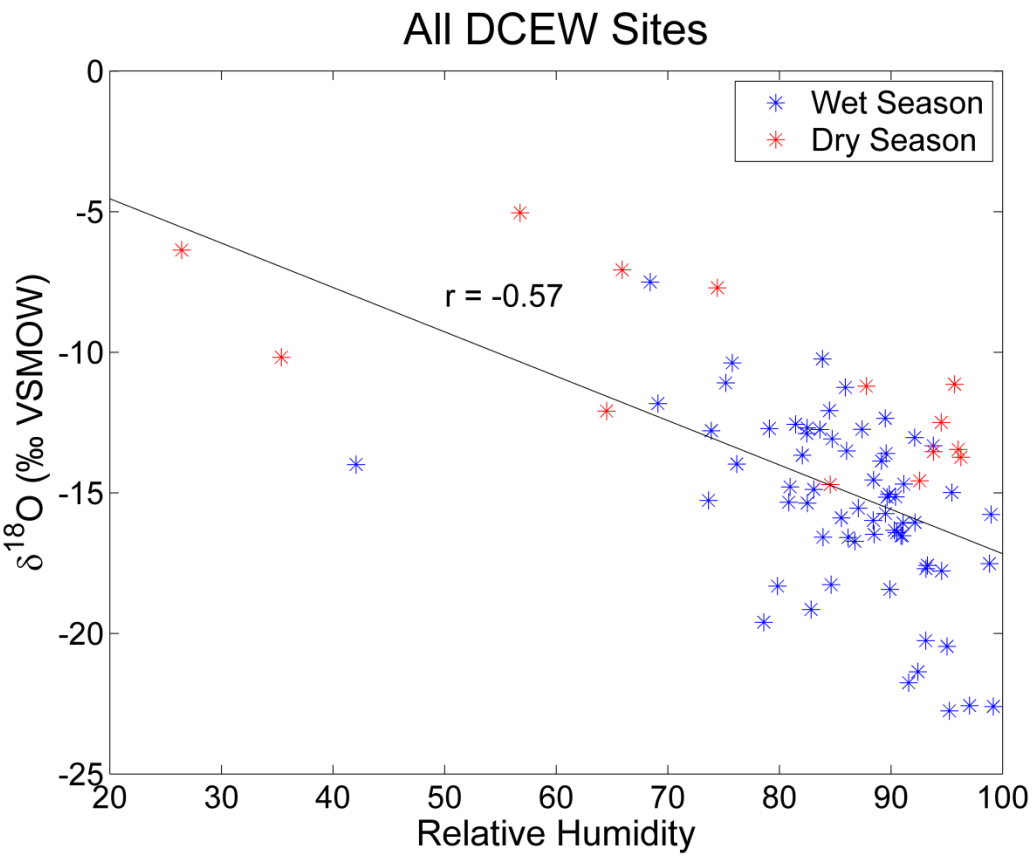

Figure 13: Relationship between $\delta^{18}O$ of precipitation and average relative humidity for each precipitation event.

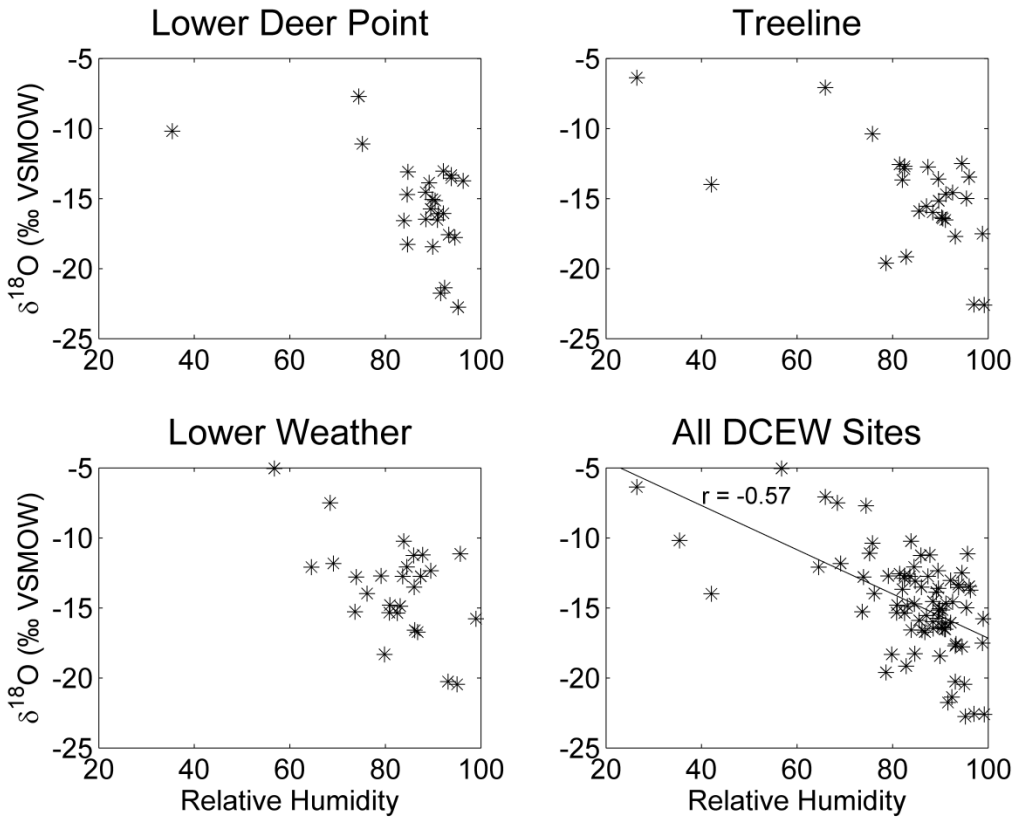

Figure 14: Relationship between $\delta^{18}O$ of precipitation and average relative humidity for each precipitation event at each collection site.

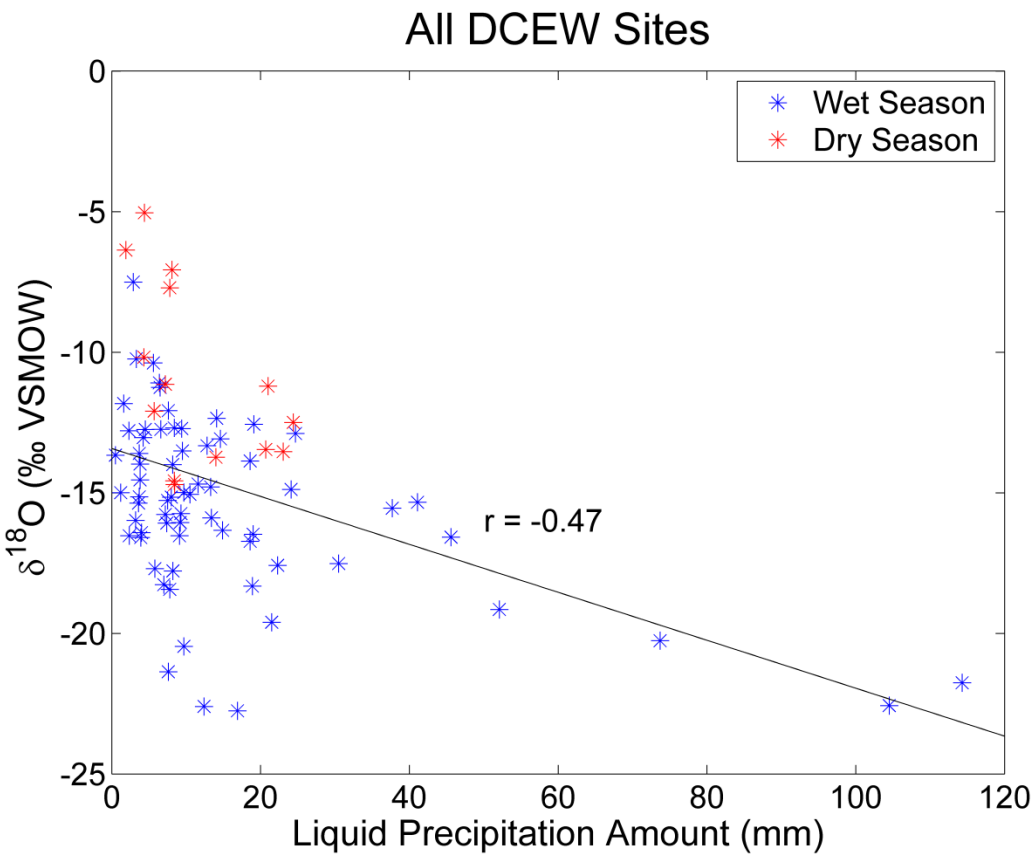

Figure 15: Relationship between $\delta^{18}O$ of precipitation and total precipitation amount (mm) for each precipitation event.

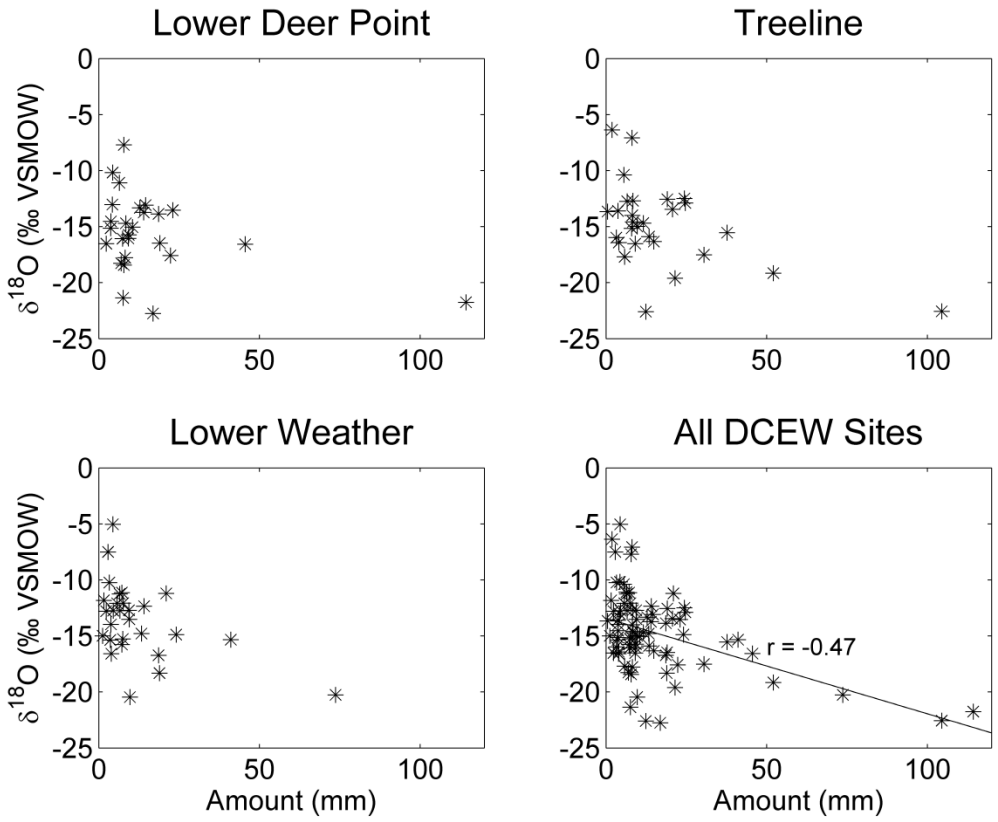

Figure 16: Relationship between $\delta^{18}O$ of precipitation and total precipitation amount (mm) for each precipitation event at each collection site.

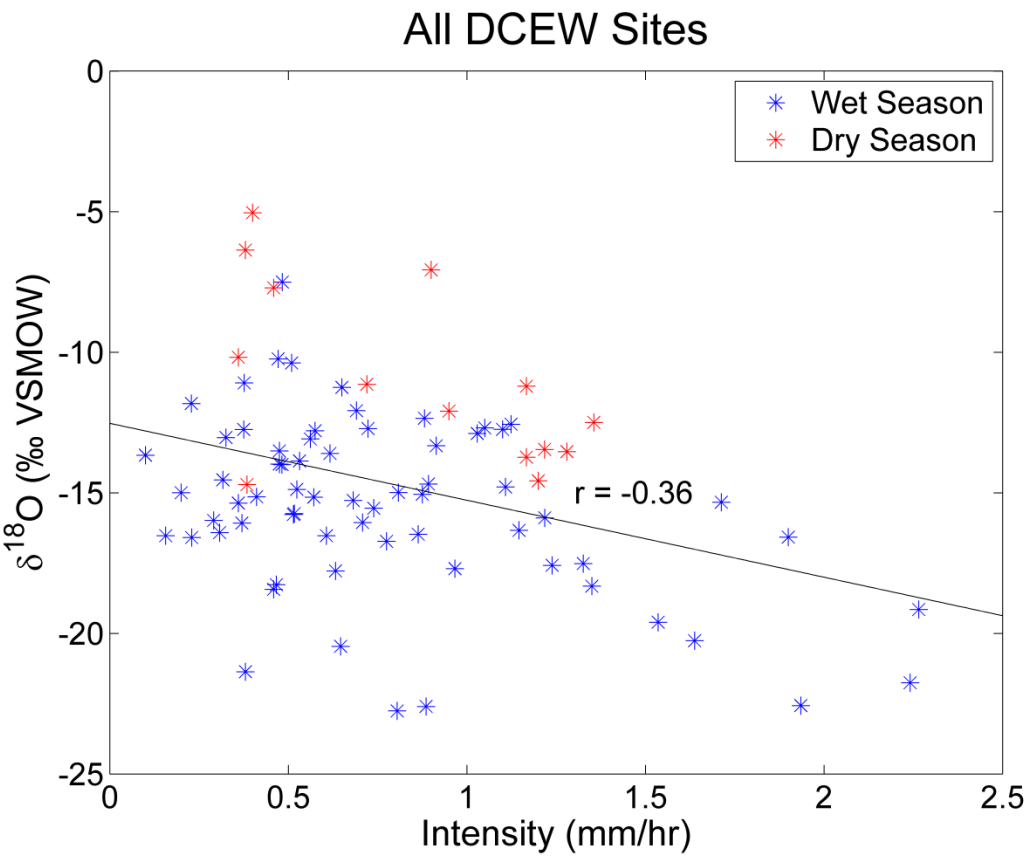

Figure 17: Relationship between $\delta^{18}O$ of precipitation and precipitation intensity (mm/hour) for each precipitation event.

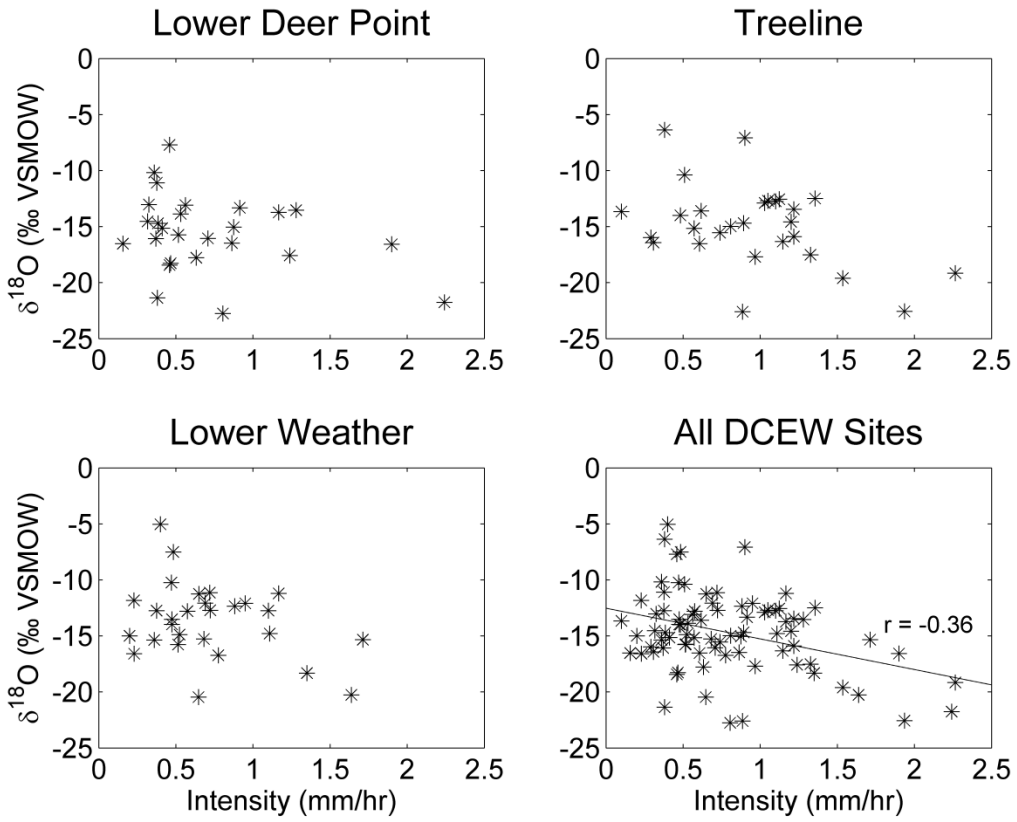

Figure 18: Relationship between $\delta^{18}O$ of precipitation and precipitation intensity (mm/hour) for each precipitation event at each collection site.

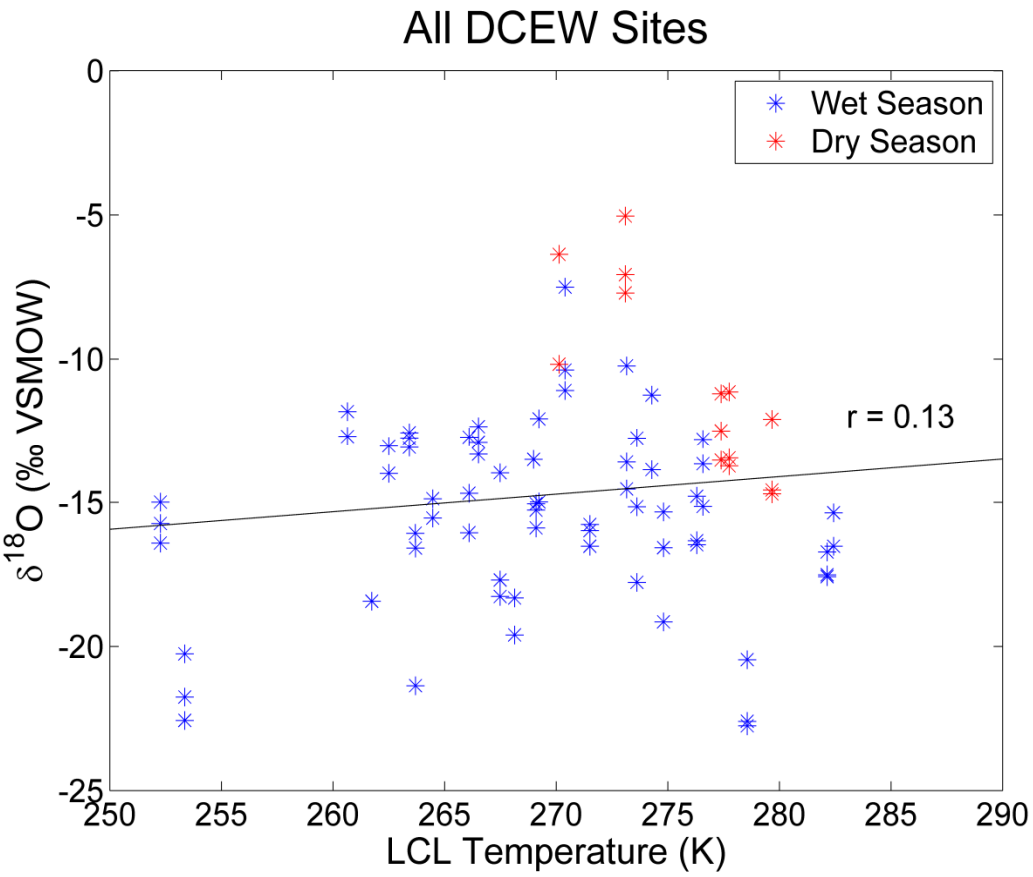

Figure 19: Relationship between $\delta^{18}O$ of precipitation and lifted condensation level temperature (K) for each precipitation event.

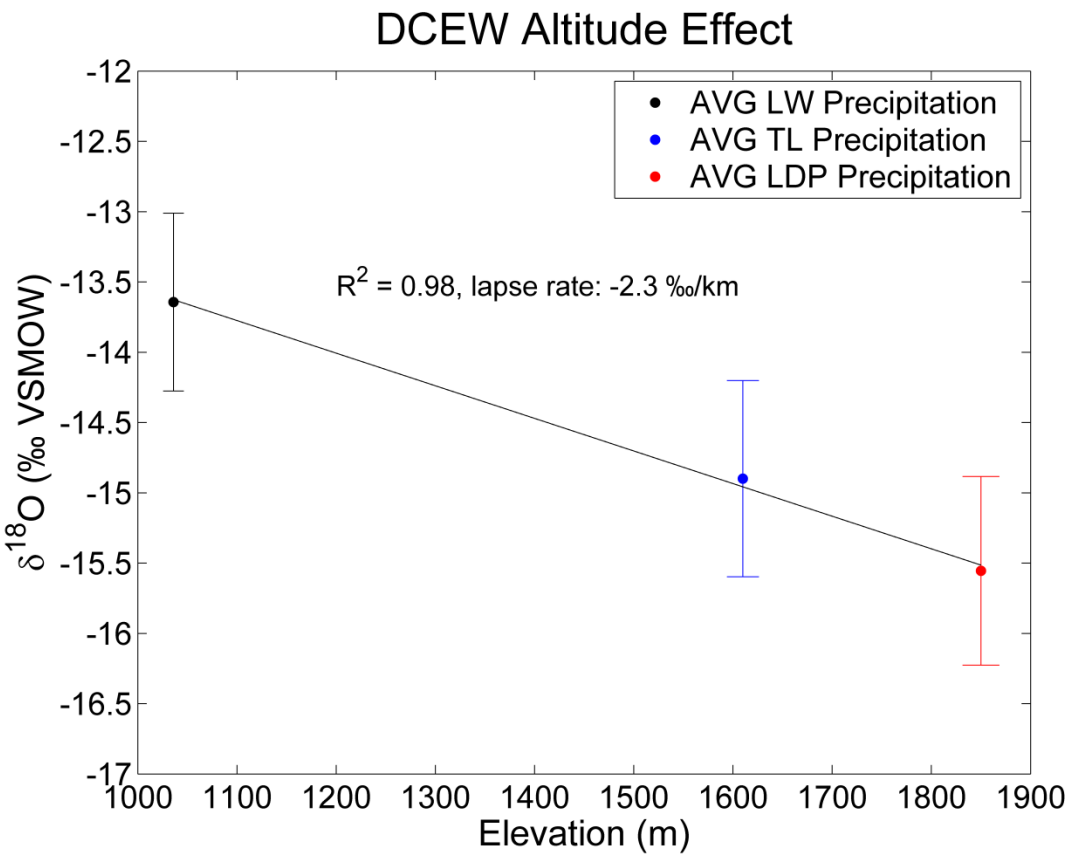

Figure 20: Relationship between the average $\delta^{18}O$ of precipitation and collection site elevation (m) for each precipitation event (May 2011 – May 2012). The Altitude effect results in an average $\delta^{18}O$ depletion of 0.22‰ /100m in Dry Creek Experimental Watershed. Error bars represent standard error of isotopic composition of precipitation at each collection site.

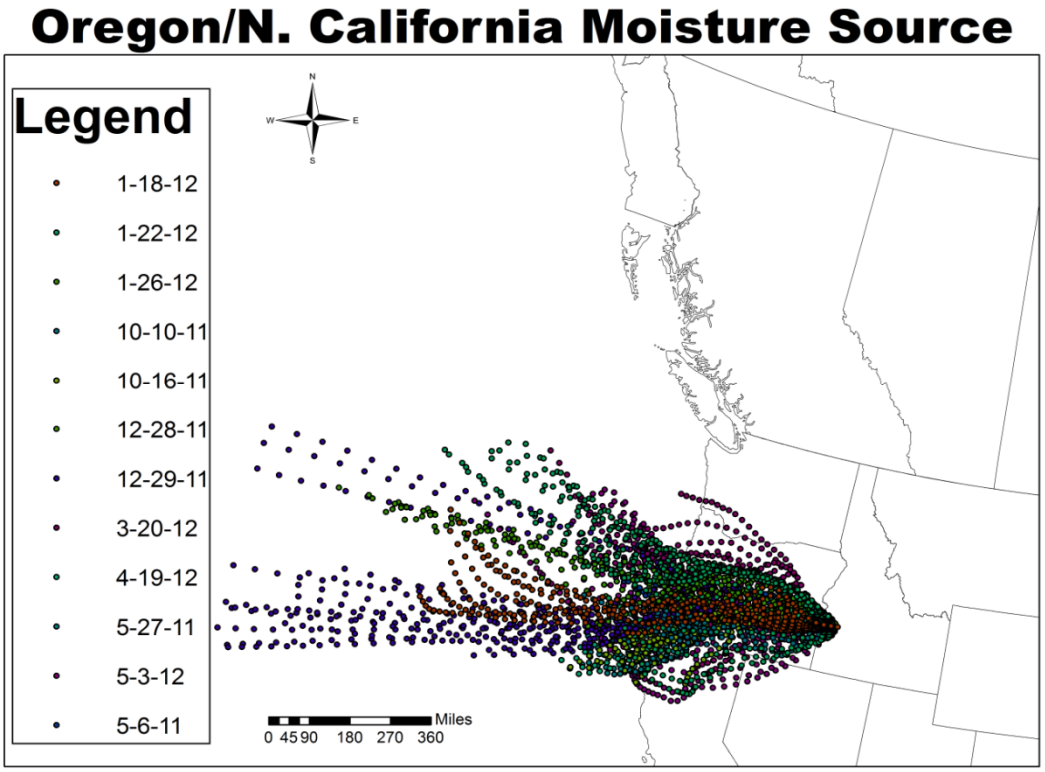

Figure 21: Precipitation events moving coastal over Oregon and Northern California based on NOAA HYSPLIT reverse trajectory analysis.

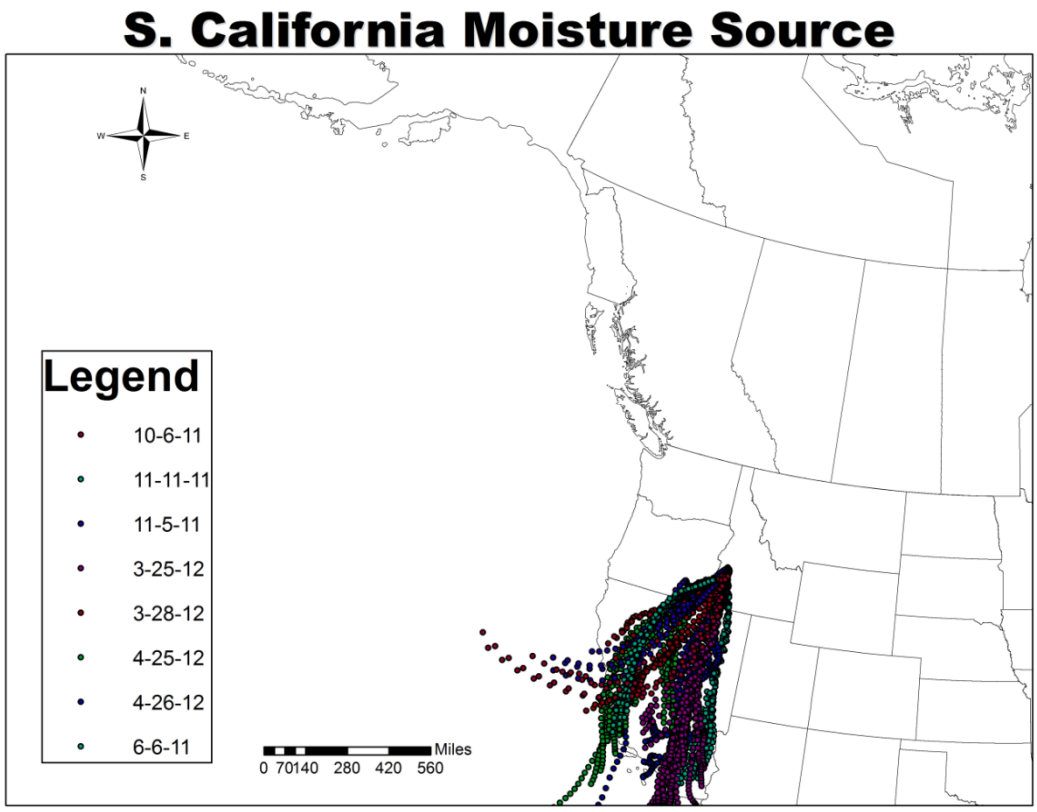

Figure 22: Precipitation events moving coastal over Southern California based on NOAA HYSPLIT reverse trajectory analysis.

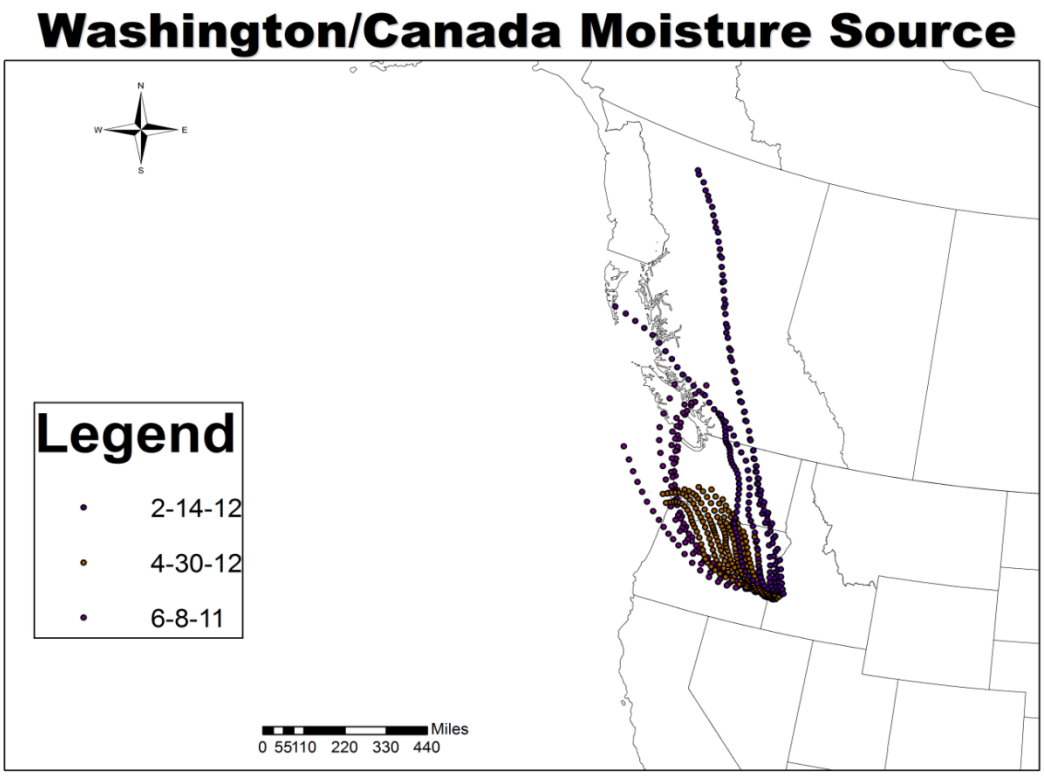

Figure 23: Precipitation events moving coastal over Canada and Washington based on NOAA HYSPLIT reverse trajectory analysis.

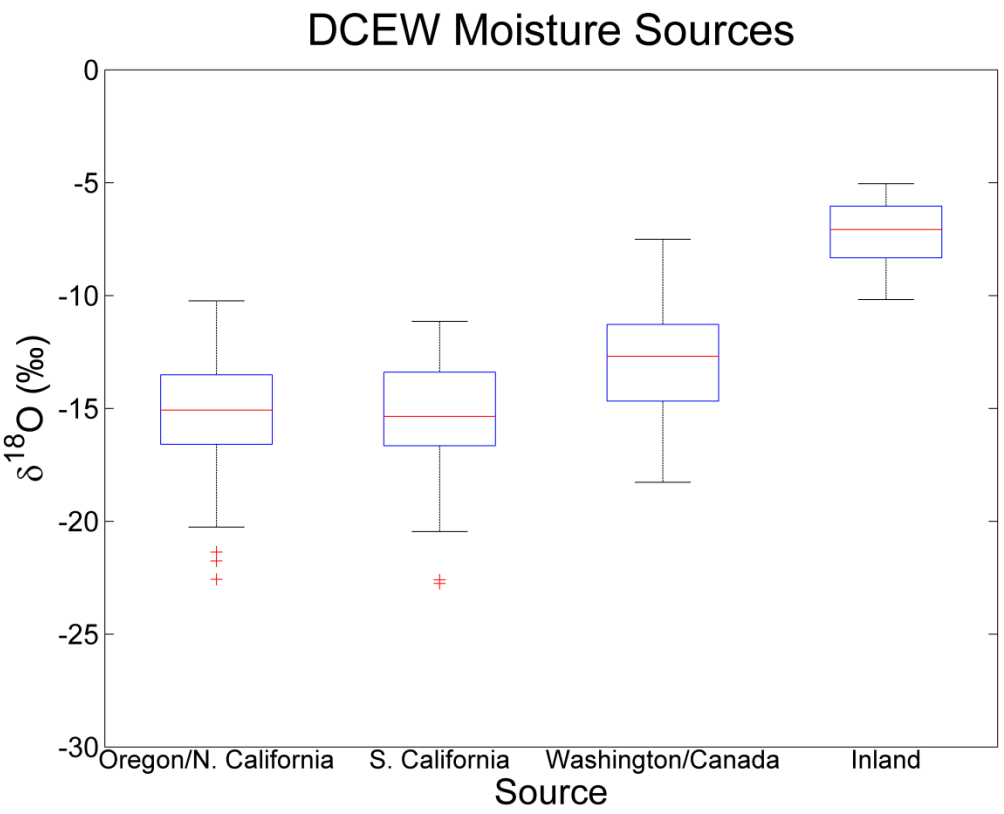

Figure 24: Box plots of $\delta^{18}O$ of precipitation from different potential moisture sources determined by NOAA HYSPLIT model.

CHAPTER TWO: THE ROLE OF SNOW IN CONTROLLING THE ISOTOPIC INPUT FUNCTION TO WATERSHEDS

1. Introduction

The input signal for transit time estimation studies is further complicated in snow-dominated catchments. Individual snow events have distinct isotopic compositions, which in large part controls the isotopic composition of the entire snowpack. However, the evolution of a snowpack changes the isotopic composition of each layer and the entire snow profile (Cooper et al. 1991). Dissimilar to rain events, snowmelt does not enter the catchment in the same chronological order in which the snow falls, which is commonly assumed in transit time estimation studies. During periods of snowmelt, isotopic fractionation related to the phase change between solid and liquid phases of water can result in melt-water with a depleted isotopic composition relative the remaining snowpack (Kendall and McDonnell 1998). The fractionation associated with melt leaves the remaining snowpack isotopically enriched and typically results in a gradual isotopic enrichment of snowmelt through the melt season (Mast et al. 1995).

Additionally, pre-melt fractionation also occurs and these processes are not inconsequential (Kendall and McDonnell 1998). Sublimation, the direct transfer of the solid to vapor phase of water, results in a snowpack with an enriched isotopic composition compared to the sublimated water vapor (Neumann et al. 2008). Vapor within the snowpack can exchange with soil water and moisture in the atmosphere, which

can alter the isotopic composition of the snowpack and tends to dilute the unique signals from individual snow events (Cooper et al. 1991). These processes, in addition to the fractionation associated with snowmelt, result in significant temporal and spatial variations of the isotopic composition of seasonal snowpacks. The true hydrological isotopic input to the catchment system is the isotopic composition of melting snow and ice through the duration of the melt season.

2. Methods and Objectives

In this study, we investigate the issue of snowpack complications in the input characterization problem by examining the spatial variation of the isotopic composition of snow. We collected snow in DCEW at the Treeline study site. The Treeline study site is a small micro-catchment that drains approximately 0.02 km^2, and typically has snow cover from December – March. The elevation of the study site is 1610 m, and all hillslope aspects are represented in the northwest to southeast trending catchment. The combination of a consistent snowpack and slopes representing all aspects make the Treeline study site a suitable location for our snow-based investigation. The data in this section are from two separate snow sampling campaigns both completed at the Treeline study site in DCEW.

During the first sampling campaign, snow samples were collected at 2 cm increments through the entirety of snow pit profiles (vertical direction) at 3 separate locations near the Treeline study site. Pit 1 was on the top of ridge trending from the northwest to southeast, leaving it exposed to all directions. Pit 2 was on a slope with a southwest-facing aspect and pit 3 was on a slope with an easterly aspect. All 3 pits were within 150 meters of each other. The sampling campaign was performed on January 27

2012, approximately 7 days after a large mixed rain-snow event that delivered <10 cm of liquid water equivalent to the Treeline weather station.

The second snow sampling campaign consisted of the collection of bulk snow core samples at the Treeline study site on an individual hillslope. Bulk snow core samples were collected with a federal sampler in a "star pattern" on the hillslope. The star pattern was associated with transects in the up/down-slope, cross-slope, and diagonal directions (Figures 25 and 26). The star sampling technique resulted in four separate 16 meter transects. Snow core samples were collected every meter along each transect, resulting in 64 total samples covering an area of approximately 256 m^2. Additionally, snow depth was measured for all 64 samples.

For both snow sampling campaigns, all snow samples were stored in zip lock plastic bags and allowed to completely melt in a refrigerator. After samples were completely melted, they were well mixed and transferred to 5 ml glass vials in preparation for isotopic analysis on the LWIA in the Stable Isotope Laboratory at Boise State University.

3. Results and Discussion

Figures 27 and 28 display the isotopic composition of snow samples ($\delta^{18}O$ and $\delta^{2}H$, respectively) plotted against the depth of collection from 3 snow pits at the Treeline study site. Pit 1, which was on a ridge top and the most exposed location to wind and solar radiation, is more isotopically enriched from the top of the snowpack to 10 cm from the ground surface. Furthermore, the depth of snow at pit 1 was less than 35 cm while the other 2 pits were greater than 40 cm. Mass losses likely occurred at this location through sublimation, melt, or wind scour. Sublimation and melt processes result in an isotopic

enrichment of the remaining snow. The extreme isotopic depletion towards the bottom of the snowpack at pit 1 could be the result of several successive melt-freeze cycles, with depleted water isotopes preferentially melting in the upper layers of the snowpack and subsequently refreezing near the ground surface.

All 3 pits display a trend of a more enriched isotopic composition towards the top of the snowpack. Other studies have observed the same trend (Rodhe 1987, Sommerfeld et al. 1991), which can result from evaporative loss of depleted isotopes through sublimation, leaving the remaining snow isotopically enriched. The precipitation event that created the snowpack for this study was a wet snow, and transitioned to rain near the end of the event. The observed enrichment trend towards the top of the snowpack in all 3 pits could also be a product of intra-storm evolution, since rain is typically more enriched relative to snow from the same event due to the increased temperature. Increased temperature results in less equilibrium fractionation during condensation (Dansgaard 1964), and the resulting raindrops have greater potential for kinetic fractionation through evaporative enrichment during decent (Mast et al. 1995).

Figure 28 displays the LMWL for the Treasure Valley area along with the isotopic composition of each sample from all 3 snow pits and the isotopic composition of the bulk precipitation sample (rain and snow) that created the snowpack. There is an observable systematic difference between pits 1 and 2 and pit 3. All samples from pit 3 plot above the LMWL, along with the bulk precipitation sample. Conversely, all samples from pits 1 and 2 plot below the LMWL.

Pits 1 and 2 were on slopes with south to southwest facing aspects and pit 3 was on an easterly facing aspect. The south to southwest aspect receives more solar radiation

and is exposed to the predominant wind direction (west) at this location. These correlating factors potentially increase the likelihood of sublimation at pits 1 and 2 relative to pit 3. Since the bulk precipitation sample plots near the line of samples from pit 3, it is plausible that fractionation associated with sublimation changed the composition of pits 1 and 2. Evaporative losses through sublimation results in an enrichment trend of both $\delta^{18}O$ and $\delta^{2}H$ (Sokratov and Golubev 2009), which could partially explain the difference between pits 1 and 2 and that at pit 3. However, the most isotopically depleted samples were also from pits 1 and 2, suggesting an additional fractionation process. The additional process could be the result of the snowpack melting and refreezing, creating a snowpack with a wider range of isotopic values, including more depleted isotopic values than the original snowpack composition.

The $\delta^{18}O$ of each bulk snow sample from the star sampling campaign is displayed in Figure 30. The $\delta^{18}O$ varied between -16 and -19 ‰, with a mean composition of -17.6 ‰. This is a substantial isotopic variation considering the spatial resolution of the sampling campaign (256 m^2) and is greater than the variation of the annual $\delta^{18}O$ of Dry Creek stream water. The y-transect variation appears to become more isotopically depleted in the downslope direction. The average $\delta^{18}O$ of the upper 8 y-direction samples is -17.53 ‰ (+/- 0.1) while the average lower 8 y-direction samples is -18.06 ‰ (+/- 0.1). Figure 31 displays the relationship between the $\delta^{18}O$ of bulk snow samples, and the y-transect location of each sample. Although data points are limited, linear regression results in a moderate to strong correlation ($r = 0.57$, $p < 0.05$).

The y-direction downslope isotopic depletion trend is not controlled by snow depth because $\delta^{18}O$ vs. depth (Figure 32) displays no correlation ($r = 0.02$). A possible

explanation for the isotopic depletion in the downslope direction is the lateral redistribution of melt-water. Recent studies have suggested the lateral redistribution of snowmelt can be significant throughout the winter (Eiriksson et al. 2013). Since the more depleted isotopes (^{16}O and ^{1}H) melt first, the remaining snowpack becomes isotopically enriched. If the melt-water is redistributed by lateral flow in the downslope direction and refreezes, the downslope snow would become isotopically depleted relative to the upslope snow. Further investigations and statistical analysis needs to be performed (e.g., longer y-direction transect, sample multiple locations, subsample dataset during analysis) to test the robustness of these conclusions.

4. Conclusions

Fractionation processes that control and change the isotopic composition of snow are complex, making it unlikely the isotopic composition of snowmelt will resemble the order in which the snowpack was created. The complication of the input signal in snow-dominated catchments is problematic for transit time estimation studies, especially when the input is considered to be the raw isotopic composition of precipitation data. Areas of catchments that receive high winds are likely to have increased sublimation rates. As a result, snow at higher elevations as well as ridges and sparsely vegetated regions (where wind speeds are presumably stronger) may undergo more sublimation than snow in lower elevation and more sheltered regions. Snowpacks in areas with enhanced sublimation could be expected to be isotopically enriched, all else being equal. In contrast to the Altitude effect, which predicts isotopic depletion of precipitation with increasing altitude, the interaction of processes that would tend to isotopically enrich or deplete precipitation

suggests substantial complexity in the spatiotemporal pattern of the isotopic input function to watersheds.

However, this complexity does not make the problem intractable and the study of the isotopic composition of evolving snow presents opportunities beyond transit time estimation studies (e.g., mass loss, vapor fluxes, melt rates, lateral flow, crystal structure alterations, etc.). Using snowmelt lysimeters to sample the isotopic composition of melt water throughout the melt season is a better way to estimate the input signal required for transit time studies. This method also has drawbacks (including increased labor and cost, as well as inherently local observations), but coupled with the techniques and methods applied here could further constrain two critical phases (precipitation and snowpack evolution) of the evolution of isotope tracers arriving in watersheds as precipitation and leaving as streamflow.

Appendix B

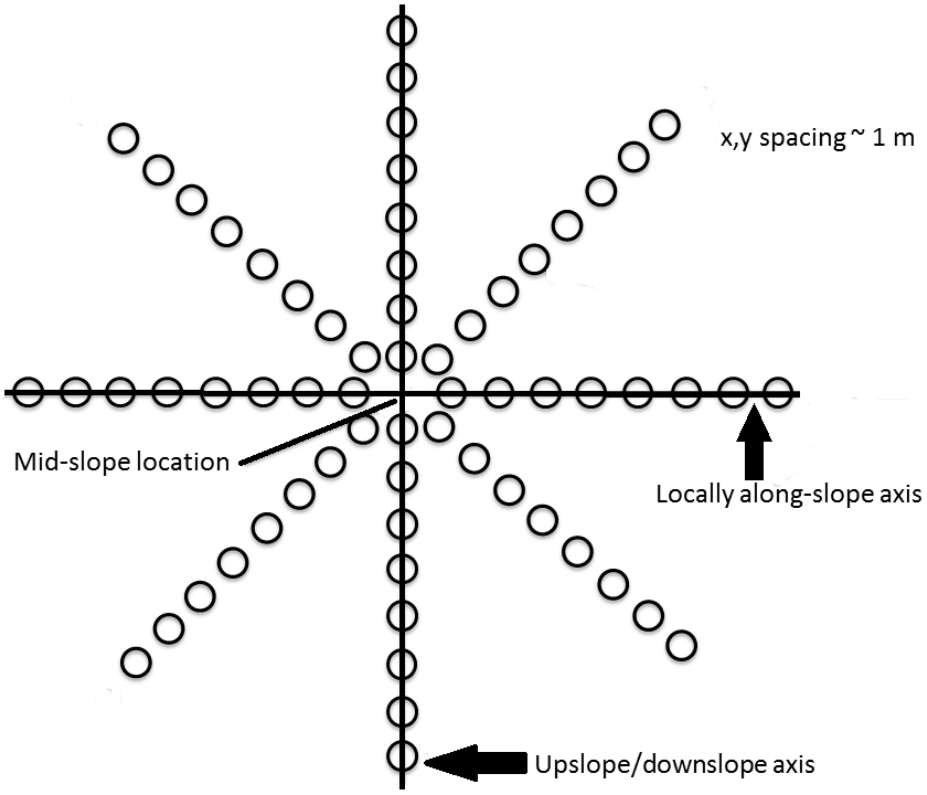

Figure 25: Snow Star sampling technique.

Figure 26: Sampling on 3-5-12 at Treeline Study Site in Dry Creek Experimental Watershed. Bulk snow-core samples were collected using a federal sampler. Elevation: 1624 meters.

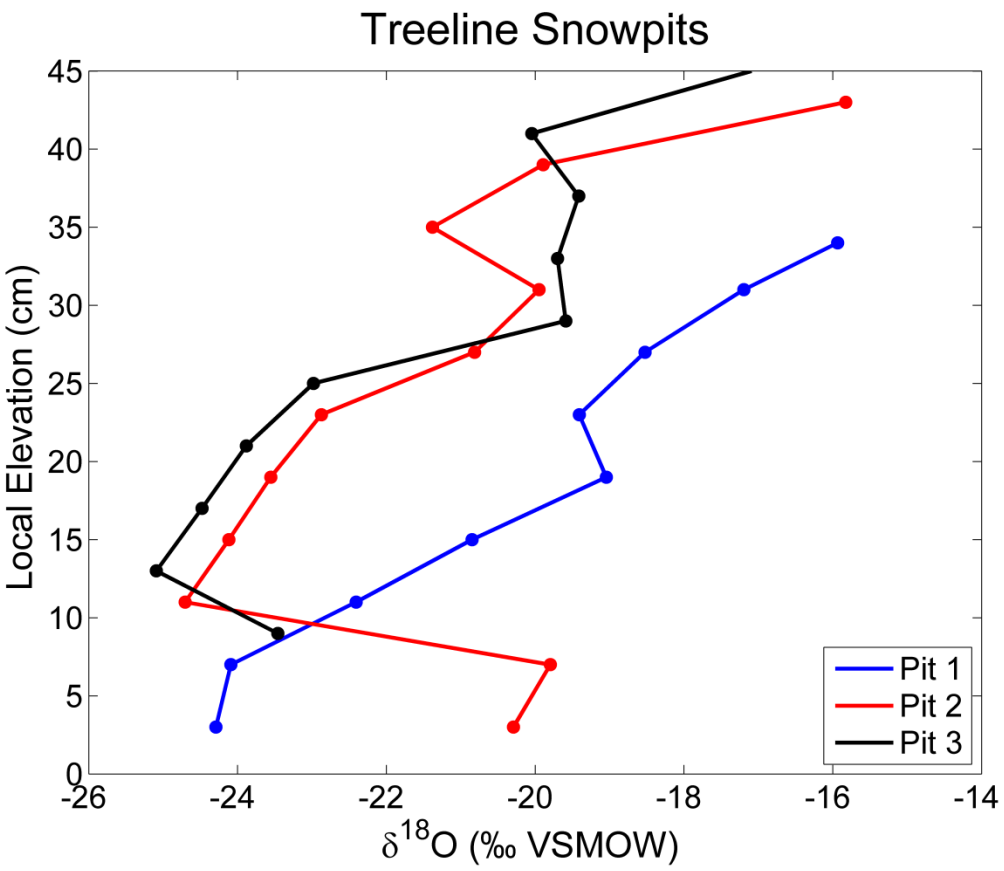

Figure 27: $\delta^{18}O$ of snow samples at 2 cm increments through entire snow profile at 3 separate locations. Pit 3 snowpit was directly over a bush, resulting in compromised samples below 9 cm.

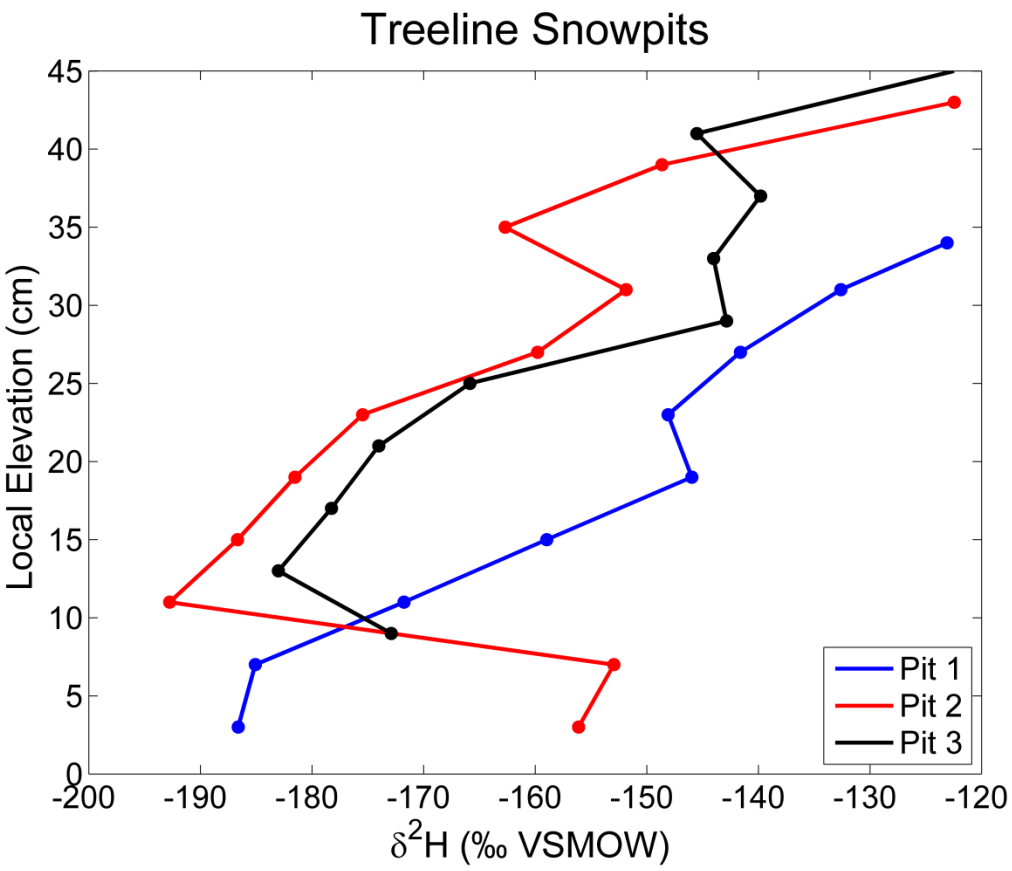

Figure 28: δ^2H of snow samples at 2 cm increments through entire snow profile at 3 separate locations. Pit 3 snowpit was directly over a bush, resulting in compromised samples below 9 cm.

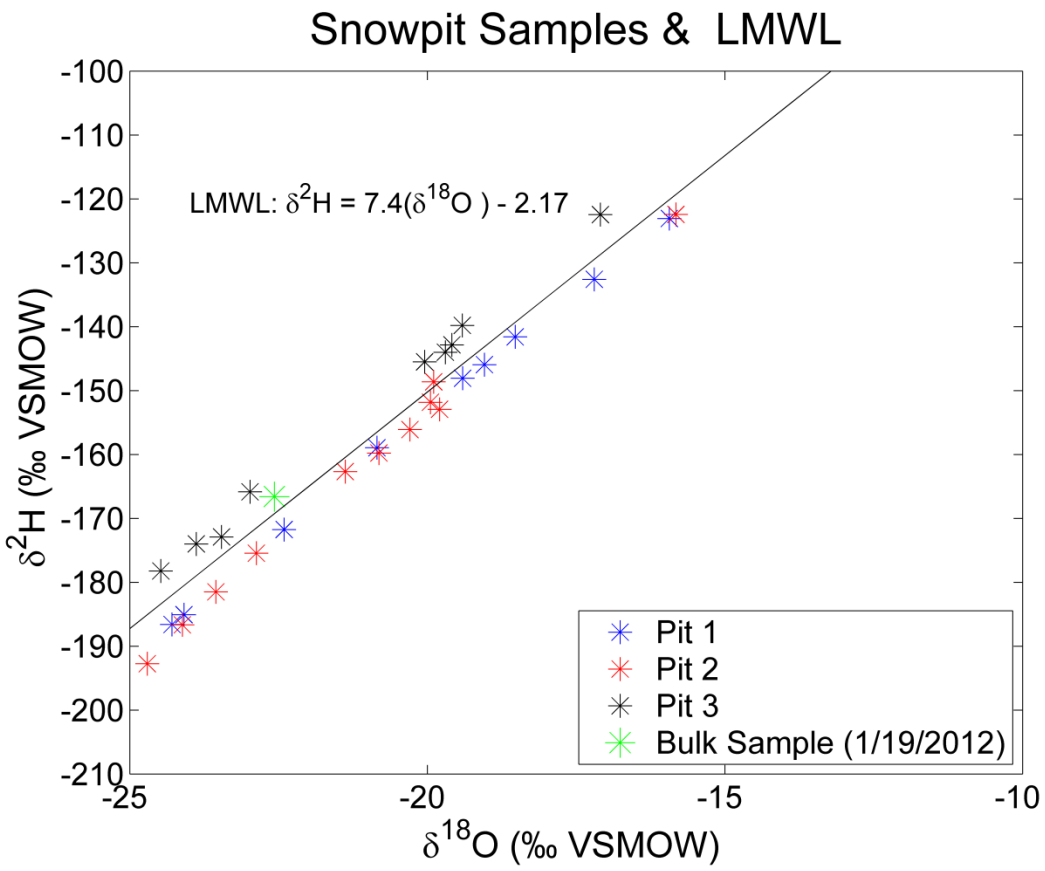

Figure 29: Isotopic composition of all 3 snowpit samples plotted with LMWL.

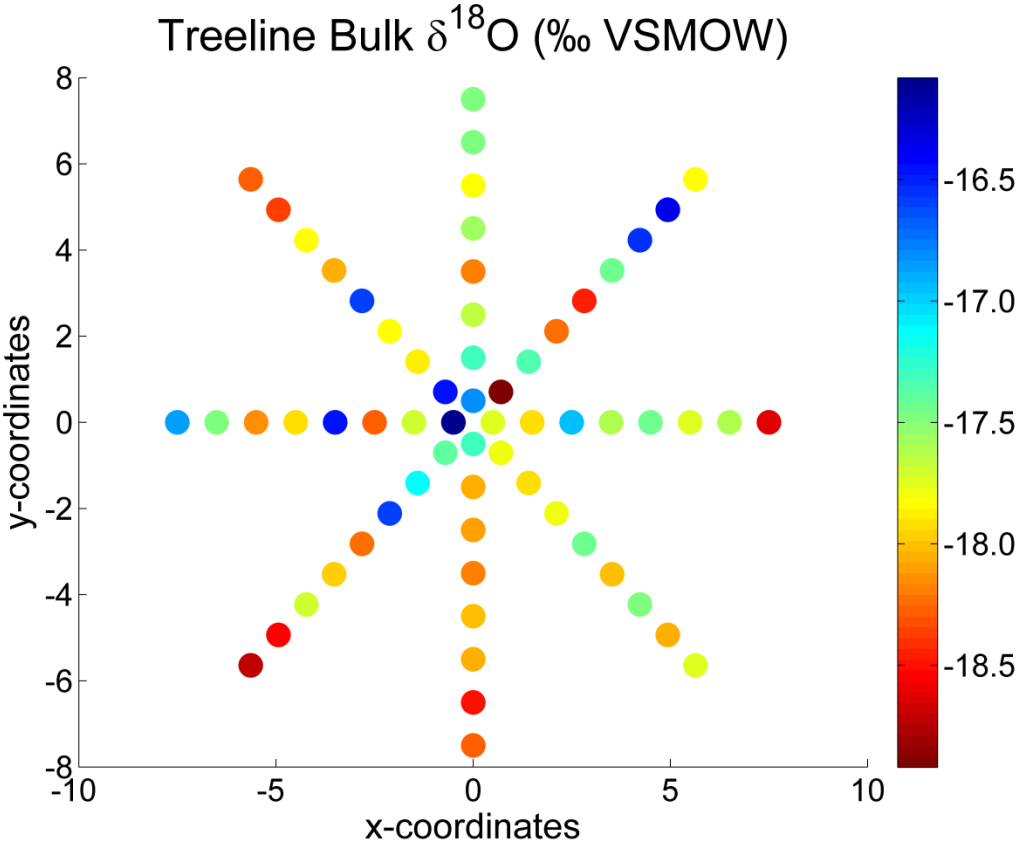

Figure 30: **$\delta^{18}O$ of bulk snow samples (1 meter spacing) at Treeline study site.**

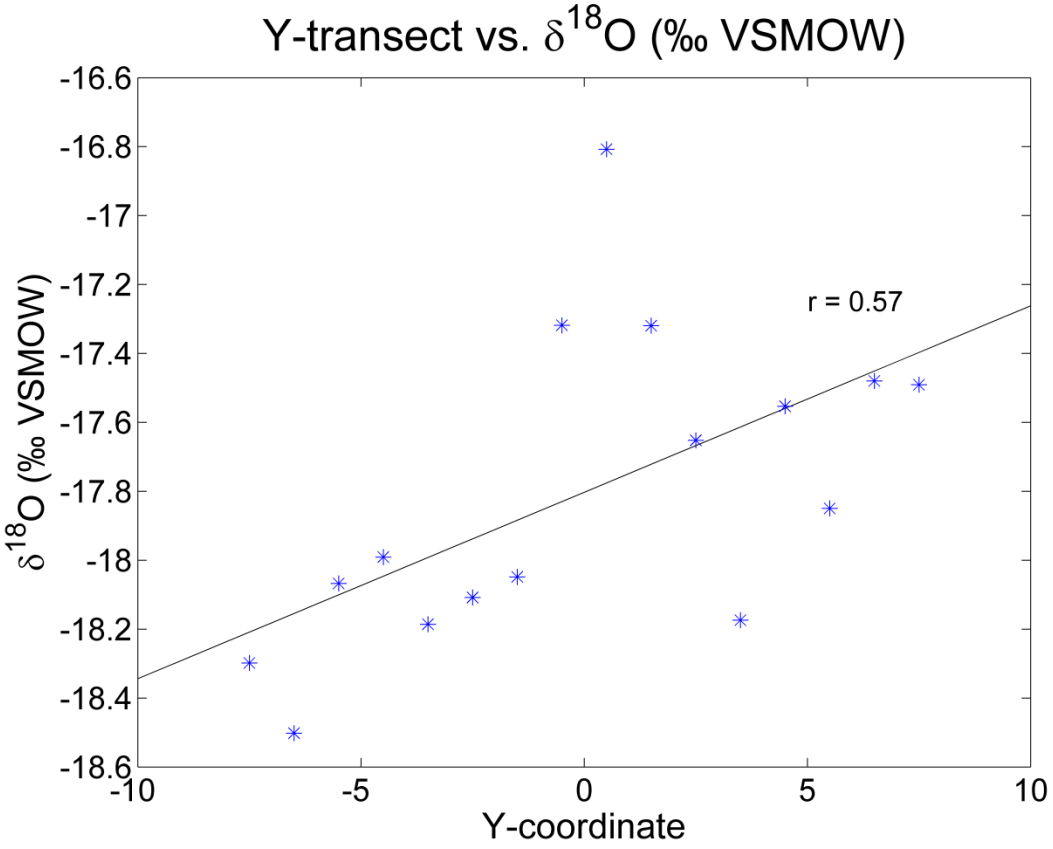

Figure 31: $\delta^{18}O$ of star technique samples plotted against Y-transect values.

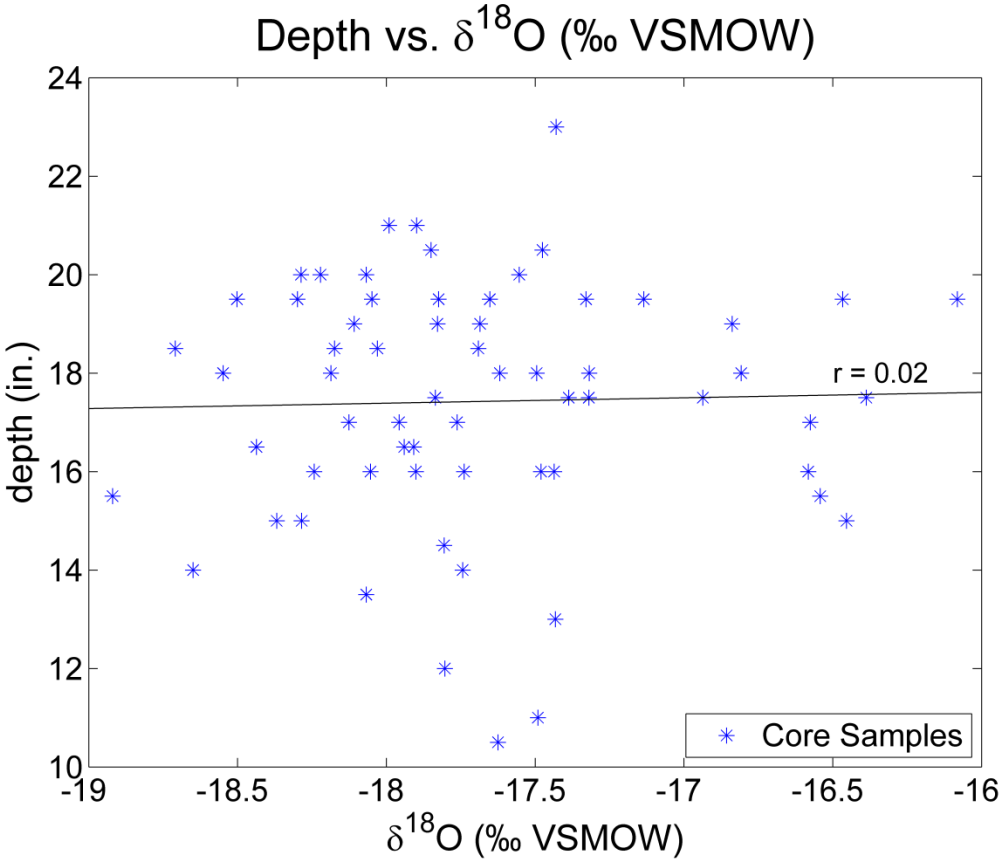

Figure 32: $\delta^{18}O$ of star technique samples plotted against the recorded snow depth of each sample.

REFERENCES

Aishlin, P. & J. P. McNamara (2011) Bedrock infiltration and mountain block recharge accounting using chloride mass balance. *Hydrological Processes,* 25**,** 1934-1948.

Ambach, W., W. Dansgaard, H. Eisner & J. Møller (1968) The altitude effect on the isotopic composition of precipitation and glacier ice in the Alps. *Tellus,* 20**,** 595-600.

Berman, E. S. F., M. Gupta, C. Gabrielli, T. Garland & J. J. McDonnell (2009) High-frequency field-deployable isotope analyzer for hydrological applications. *Water Resources Research,* 45**,** W10201.

Bograd, S., F. Schwing, R. Mendelssohn & P. Green-Jessen (2002) On the changing seasonality over the North Pacific. *Geophysical research letters,* 29**,** 1333.

Brand, W. A., H. Geilmann, E. R. Crosson & C. W. Rella (2009) Cavity ring-down spectroscopy versus high-temperature conversion isotope ratio mass spectrometry; a case study on δ2H and δ18O of pure water samples and alcohol/water mixtures. *Rapid Communications in Mass Spectrometry,* 23**,** 1879-1884.

Breitenbach, S. F. M., J. F. Adkins, H. Meyer, N. Marwan, K. K. Kumar & G. H. Haug (2010) Strong influence of water vapor source dynamics on stable isotopes in

precipitation observed in Southern Meghalaya, NE India. *Earth and Planetary Science Letters,* 292**,** 212-220.

Burnett, A. W., H. T. Mullins & W. P. Patterson (2004) Relationship between atmospheric circulation and winter precipitation δ18O in central New York State. *Geophysical research letters,* 31**,** L22209.

Clark, I. D. & P. Fritz. 1997. *Environmental isotopes in hydrogeology*. CRC.

Cooper, L. W., C. R. Olsen, D. K. Solomon, I. L. Larsen, R. B. Cook & J. M. Grebmeier (1991) Stable isotopes of oxygen and natural and fallout radionuclides used for tracing runoff during snowmelt in an Arctic watershed. *Water Resources Research,* 27**,** 2171-2179.

Coplen, T. B., A. L. Herczeg & C. Barnes. 2000. Isotope engineering–using stable isotopes of the water molecule to solve practical problems. 79-110. Kluwer Academic Publishers: Boston.

Craig, H. (1961) Isotopic variations in meteoric waters. *Science (New York, NY),* 133**,** 1702.

Craig, H. & L. I. Gordon. 1965. *Deuterium and oxygen 18 variations in the ocean and the marine atmosphere*. Consiglio nazionale delle richerche, Laboratorio de geologia nucleare.

Dansgaard, W. (1964) Stable isotopes in precipitation. *Tellus,* 16**,** 436-468.

Dansgaard, W., S. J. Johnsen, H. B. Clausen, D. Dahl-Jensen, N. S. Gundestrup, C. U. Hammer, C. S. Hvidberg, J. P. Steffensen, A. E. Sveinbjörnsdottir & J. Jouzel

(1993) Evidence for general instability of past climate from a 250-kyr ice-core record. *Nature,* 364**,** 218-220.

Draxler, R. R. & G. D. Rolph. 2003. HYSPLIT (HYbrid Single-Particle Lagrangian Integrated Trajectory) model access via NOAA ARL READY website (http://www. arl. noaa. gov/ready/hysplit4. html). NOAA Air Resources Laboratory, Silver Spring. Md.

Dutton, A., B. H. Wilkinson, J. M. Welker, G. J. Bowen & K. C. Lohmann (2005) Spatial distribution and seasonal variation in 18O/16O of modern precipitation and river water across the conterminous USA. *Hydrological Processes,* 19**,** 4121-4146.

Eiriksson, D., M. Whitson, C. H. Luce, H. P. Marshall, J. Bradford, S. G. Benner, T. Black, H. Hetrick & J. P. McNamara (2013) An evaluation of the hydrologic relevance of lateral flow in snow at hillslope and catchment scales. *Hydrological Processes*.

Fricke, H. C. & J. R. O'Neil (1999) The correlation between< sup> 18</sup> O/< sup> 16</sup> O ratios of meteoric water and surface temperature: its use in investigating terrestrial climate change over geologic time. *Earth and Planetary Science Letters,* 170**,** 181-196.

Friedman, I. (1953) Deuterium content of natural waters and other substances. *Geochimica et Cosmochimica Acta,* 4**,** 89-103.

Goldsmith, G. R., L. E. Muñoz-Villers, F. Holwerda, J. J. McDonnell, H. Asbjornsen & T. E. Dawson (2011) Stable isotopes reveal linkages among ecohydrological processes in a seasonally dry tropical montane cloud forest. *Ecohydrology*.

Henderson-Sellers, A., K. McGuffie, D. Noone & P. Irannejad (2004) Using stable water isotopes to evaluate basin-scale simulations of surface water budgets. *Journal of Hydrometeorology,* 5**,** 805-822.

Henderson-Sellers, A. & P. J. Robinson. 1986. *Contemporary climatology*. Longman Scientific & Technical.

Hoefs, J. 2009. *Stable isotope geochemistry*. Springer.

Kendall, C. & J. J. McDonnell. 1998. *Isotope tracers in catchment hydrology*. Elsevier Science Limited.

Kirby, M. E., H. T. Mullins, W. P. Patterson & A. W. Burnett (2002) Late glacial–Holocene atmospheric circulation and precipitation in the northeast United States inferred from modern calibrated stable oxygen and carbon isotopes. *Geological Society of America Bulletin,* 114**,** 1326-1340.

Lawrence, J. R., S. D. Gedzelman, J. W. C. White, D. Smiley & P. Lazov (1982) Storm trajectories in eastern US D/H isotopic composition of precipitation.

Lee, J. E., I. Fung, D. J. DePaolo & C. C. Henning (2007) Analysis of the global distribution of water isotopes using the NCAR atmospheric general circulation model. *Journal of Geophysical Research,* 112**,** D16306.

Lee, K. S., A. J. Grundstein, D. B. Wenner, M. S. Choi, N. C. Woo & D. H. Lee (2003) Climatic controls on the stable isotopic composition of precipitation in North-east Asia. *Climate Research,* 23**,** 137-148.

Mast, M.A., C. Kendall, D.H. Campbell, D.W. Clow, J. Back (1995) Determination of hydrologic pathways in an alpine-subalpine basin using isotopic and chemical

tracers. *Biogeochemistry of Seasonally Snow-Covered Catchments,* International Association of Hydrological Sciences, 263-270

McDonnell, J. J., K. McGuire, P. Aggarwal, K. J. Beven, D. Biondi, G. Destouni, S. Dunn, A. James, J. Kirchner & P. Kraft (2010) How old is streamwater? Open questions in catchment transit time conceptualization, modelling and analysis. *Hydrological Processes,* 24**,** 1745-1754.

McGuire, K. J. & J. J. McDonnell (2006) A review and evaluation of catchment transit time modeling. *Journal of Hydrology,* 330**,** 543-563.

McNamara, J. P., D. Chandler, M. Seyfried & S. Achet (2005) Soil moisture states, lateral flow, and streamflow generation in a semi-arid, snowmelt-driven catchment. *Hydrological Processes,* 19**,** 4023-4038.

Merlivat, L. & J. Jouzel (1979) Global climatic interpretation of the deuterium-oxygen 18 relationship for precipitation. *Journal of Geophysical Research,* 84**,** 5029-5033.

Moe, C. L. & R. D. Rheingans (2006) Global challenges in water, sanitation and health. *Journal of water and health,* 4**,** 41.

National Weather Service (2012) http://weather.noaa.gov (accessed December 2012)

Neumann, T. A., M. R. Albert, R. Lomonaco, C. Engel, Z. Courville & F. Perron (2008) Experimental determination of snow sublimation rate and stable-isotopic exchange. *Annals of Glaciology,* 49**,** 1-6.

Peng, H., B. Mayer, S. Harris & H. Krouse (2007) The influence of below-cloud secondary effects on the stable isotope composition of hydrogen and oxygen in precipitation at Calgary, Alberta, Canada. *Tellus B,* 59**,** 698-704.

Petit, J. R., J. Jouzel, D. Raynaud, N. I. Barkov, J. M. Barnola, I. Basile, M. Bender, J. Chappellaz, M. Davis & G. Delaygue (1999) Climate and atmospheric history of the past 420,000 years from the Vostok ice core, Antarctica. *Nature,* 399**,** 429-436.

Pfahl, S. & H. Wernli (2008) Air parcel trajectory analysis of stable isotopes in water vapor in the eastern Mediterranean. *Journal of Geophysical Research,* 113**,** D20104.

Poage, M. A. & C. P. Chamberlain (2001) Empirical relationships between elevation and the stable isotope composition of precipitation and surface waters: considerations for studies of paleoelevation change. *American Journal of Science,* 301**,** 1-15.

Rodhe, A. 1987. The origin of streamwater traced by oxygen-18. Uppsala University, Department of Physical Geography, Division of Hydrology.

Rogers, E., Y. Lin, K. Mitchell, W. Wu, B. Ferrier, G. Gayno, M. Pondeca, M. Pyle, V. Wong & M. Ek. 2005. The NCEP North American mesoscale modeling system: final eta model/analysis changes and preliminary experiments using the WRF-NMM. In *Preprints, 21st Conf. on Wea. Analysis and Forecasting/17th Conf. on Numerical Wea. Prediction, Washington, DC, Amer. Meteor. Soc., CD-ROM B*.

Rozanski, K., L. Araguas-Araguas, R. Gonfiantini (1992) Relation between long-term trends of oxygen-18 isotope compostion of precipitation and climate. *Science*, 258, 981-985.

Sjostrom, D. J. & J. M. Welker (2009) The influence of air mass source on the seasonal isotopic composition of precipitation, eastern USA. *Journal of Geochemical Exploration,* 102**,** 103-112.

Sokratov, S. A. & V. N. Golubev (2009) Snow isotopic content change by sublimation. *Journal of Glaciology,* 55**,** 823-828.

Sommerfeld, R. A., C. Judy & I. Friedman (1991) Isotopic changes during the formation of depth hoar in experimental snowpacks. *Stable isotope geochemistry; a tribute to Samuel Epstein***,** 205-209.

Smith, T.J., J. P. McNamara, A.N. Flores, M.M. Gribb, P.S. Aishlin, S.G. Benner (2011) Small soil storage capacity limits benefit of winter snowpack to upland vegetation. *Hydrological Processes*, 25, 3858-3865.

Strong, M., Z. D. Sharp & D. S. Gutzler (2007) Diagnosing moisture transport using D/H ratios of water vapor. *Geophysical research letters,* 34**,** L03404.

Welker, J. M. (2000) Isotopic (δ18O) characteristics of weekly precipitation collected across the USA: an initial analysis with application to water source studies. *Hydrological Processes,* 14**,** 1449-1464.